Investigating the scaling effects on blade structural characteristics of wind turbine using CFD simulation

Major project-II

Submitted to Delhi Technological University in partial fulfilment of the requirement for the award of Degree of

Master of Technology

In

Renewable Energy Technology

SUBMITTED BY-

PIYUSH RAJ

2K15/RET/11

UNDER SUPERVISION OF

Prof. RAJESH KUMAR

PROFESSOR

Department of Mechanical Engineering

Delhi Technological University

(Formerly DELHI COLLEGE OF ENGINEERING)

Bawana road, Delhi -110042

CERTIFICATE

DELHI TECHNOLOGICAL UNIVERSITY

(Formerly DELHI COLLEGE OF ENGINEERING)

This is to certify that report entitled **"Investigating the scaling effects on blade structural characteristics of wind turbine using CFD simulation" by PIYUSH RAJ** in the requirement of the partial fulfilment for the award of Degree of **Master of Technology (M. Tech)** in **Renewable Energy Technology** at **Delhi Technological University**. This work was completed under my supervision and guidance.

Prof. RAJESH KUMAR

(Professor)

Delhi technological university

Delhi

DECLARATION

I, Piyush Raj, hereby certify that the work which is being presented in this thesis entitled "Investigating the scaling effects on blade structural characteristics of wind turbine using CFD simulation", is submitted in the partial fulfilment of the requirement for degree of Master of Technology (Renewable Energy Technology) in Department of Mechanical Engineering at Delhi Technological University is an authentic record of my own work carried out under the supervision of Prof. Rajesh Kumar. The matter presented in this thesis has not been submitted in any other University/Institute for the award of Master of Technology Degree. Also, it has not been directly copied from any source without giving its proper reference.

This report does not, to the best of my knowledge, contain part of my work which has been submitted for the award of any other degree either of this university or any other university without proper citation.

Date:

Place: DTU, Delhi Signature of candidate

ACKNOWLEDGEMENT

First, I would like to express my gratitude to God for giving me ideas and strengths to make my dreams true and accomplish this thesis.

To achieve success in any work, guidance plays an important role. It makes us put right amount of energy in the right direction and at right time to obtain the desired result. Express my sincere gratitude to my guide, Prof**. Rajesh Kumar**, Professor, Mechanical Engineering Department for giving valuable guidance during the course of this work, for his ever encouraging and timely moral support.

I am greatly thankful to Prof**. Vipin**, Professor and Head, Mechanical Engineering Department, Delhi Technological University, for his encouragement and inspiration for execution of this work. I express my feelings of thanks to the entire faculty and staff, Department of Mechanical Engineering, Delhi Technological University, and Delhi for their help, inspiration and moral support, which went a long way in the successful completion of my report work.

PIYUSH RAJ

(Roll No-2K15/RET/11)

ABSTRACT

Wind turbines are used in a variety of applications with different performance requirements. Investigating the influence of scaling on wind turbine characteristics can pave the way to utilize the experience gained from a smaller turbine for a larger one. In this paper, the effects of wind turbine size on structural characteristics of a rotor blade are examined using CFD simulation. A GE's 1.5 MW wind turbine was then chosen as a large turbine and a scaled down model of its rotor was simulated numerically. The results of the simulation were introduced to Similarity Theory relations in order to predict the structural characteristics of the 1.5 MW wind turbine. The 1.5 MW turbine was also simulated and the results of the simulation were compared to predictions of Similarity Theory. It was observed that the results of the simulation completely follow the values predicted by Similarity Theory. Both Similarity Theory predictions and simulation results demonstrated that the moment and mass increases with the cube of change in rotor diameter whereas the force reaction and equivalent stress grow with the square of change in diameter.

CONTENTS

LIST OF FIGURES

LIST OF TABLE

NOMENCLATURE

ABL	Atmospheric boundary layer
FEM	Finite Element Method
FSI	Fluid-Structure Interface
HAWT	Horizontal Axis Wind Turbine
VAWT	Vertical Axis Wind Turbine
NREL	National Renewable Energy Laboratory
SST	Small Scale Turbine
LST	Large Scale Turbine
RANS	Reynolds-Averaged Navier-Stokes
RNG	Renormalization Group
CFD	Computational Fluid Dynamics
BEM	Blade Element Method
k	Turbulent Kinetic energy (m^2s^2)
ε	Rate of dissipation of turbulent kinetic energy (W/kg)
ω	turbulence frequency
μ	Dynamic Viscosity(N-s/m^2)
σ	Stress (MPa)
ρ	Density (Kg/m^3
τ	Shear stress (MPA)
υ	Kinematic Viscosity (m^2/s)
λ	Tip speed ratio
ω	Specific dissipation rate

a	Axial induction factor
C_L	Lift coefficient
C_D	Drag coefficient
S	Strain rate
F	Wind speed probability
c	Weibull parameter
U	Wind velocity (m/s^2)
A	Swept area of rotor (m^2)
Re	Reynold number
u	Mean velocity (m/s^2)
T	Thrust (m)
P	Power (W)
P_{avail}	Available power (W)
T_{avail}	Thrust available (N)
u(t)	Fluctuation in wind velocity (m/s^2)
C_T	Thrust Coefficient
z_0	Roughness length
D_ω	Cross-diffusion
a_1	Closure coefficient
F_2	Second blending function

CHAPTER 1

INTRODUCTION

With the fast exhaustion of energy resources on earth which mainly includes non-renewable energy such as fossil fuels, wind energy in considered to the one of the prominent alternative energy sources which is widely accepted worldwide. Market analysis shows continuous upscaling of wind turbines, still there are various challenge regarding technical and economic feasibility of large scale wind turbines. If somehow, we can utilise the experience of small scale turbine in developing large scale turbine, we can succeed in saving a lot of amount and time which would have taken to start building large scale turbine from the scratch. It will be significant to test a scaled down model in a wind tunnel to analyse its various characteristics of to be designed large scale turbine and consequently decrease risks. In future as shown in fig 1.1, wind power capacity is expected to grow at a yearly rate of 8%, which will increase its installed capacity to 600 GW by 2018. As we move ahead for the advancement of this sector, one of the major challenges, we got to face here is to make wind energy technology economically competitive to those of non-renewable energy like oil, coal and gas.

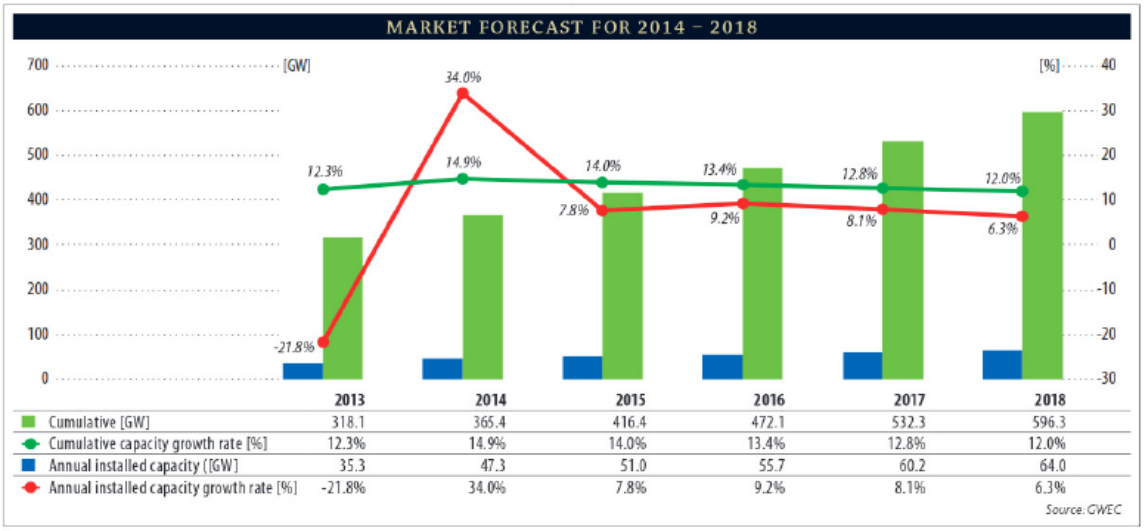

Figure 1.1 Worldwide wind power installed capacity prediction. Courtesy [1]

First step in this direction is to reduce the levelized cost of energy where the term "levelized" is defined as the cost of energy distributed for complete life of an energy system. Apparently, LCOE is the minimum price of energy at which it is sold such that it comes at a stage of no profit no loss, i.e. break-even point. This figure can be defined as the ratio of operations and maintenance of an energy system to the complete energy coverage of its system in lifetime. Further as shown in fig 1.2, in order to reduce the levelized cost of energy, we tend to increase the rotor diameter of the turbine which further leads to increment of installation height and turbine power. Larger turbines tend to extract more energy from wind but it also increases the O & M cost, but overall levelized cost decreases.

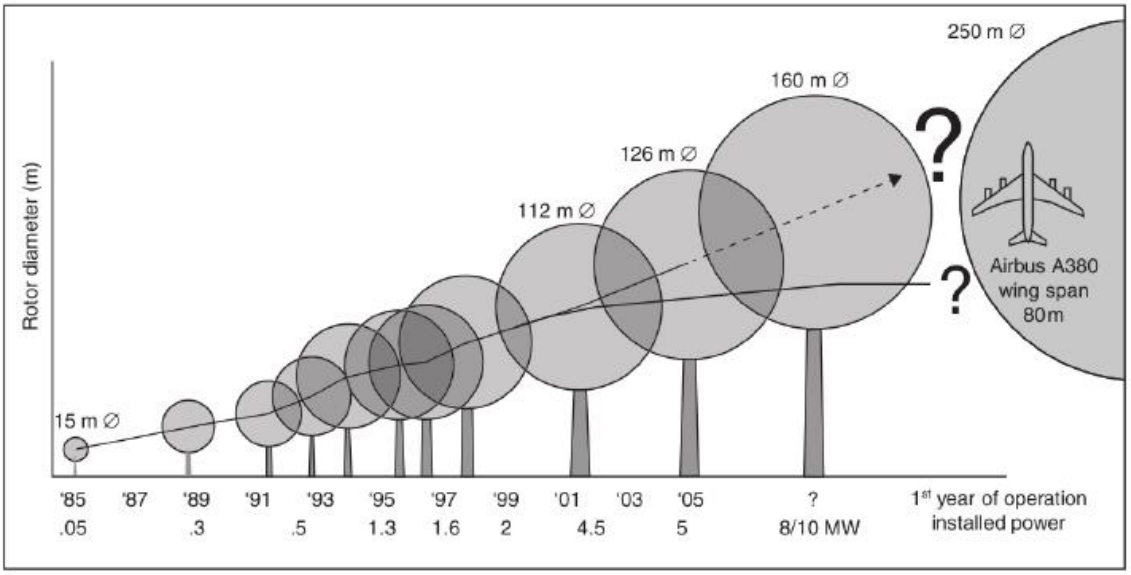

Fig 1.2 Wind turbine upscaling pattern. It shows the trends of past 3 decades in turbine power, rotor diameter and installation height. Image reproduced from [2]

If we look out for further increase of the wind turbine size, new doors can be opened for future development of wind turbine technologies [3]. However, these directions will produce new challenges in market which will require new solutions to tackle them. As shown by Ashuri [3], upscaling of large scale turbines through current scaling methods poses various technical and economic challenges for turbines close to 10 MW. Extreme and fatigue loads sustained by structural components [4] of very large turbines throughout their lifespan can be very severe which can be very dangerous. Increasing blade size can lead to increase in blade mass and other components which can be another barrier in technical feasibility and economical aspects of wind turbines. Hence, we can say that it is not possible to design large turbines just by upscaling it without considering advancement in their design to tackle problems regarding increasing blade weight etc. That's why, in recent times, there is a lot of in depth research going on for the design of more efficient turbines and not just which focuses of all aspects rather than just upscaling of turbines. For this purpose, latest analysis technologies and design methods have been developed to provide excellent understanding of operational behaviour of wind turbines

and enable designers to produce better design methods. In this thesis, it concentrates on effects of scaling on wind turbine blade structural characteristics of such as Force reaction, blade mass, equivalent stresses and moment.

In the last two decades, rapid expansion has been observed in wind turbine industry which is positive for this growing industry. Many well-known and established industries are into this sector which install wind turbines both offshore and onshore. For wind turbine energy to sustain in this market and be viable, manufacturers need to reduce the manufacturing cost of energy production in comparison to alternative energy sources. One major solution for this is to produce large rotors to generate more energy with same input and reduce the maintenance cost per megawatt output and hence, reduce cost. In fig. 1.3 shown below, offshore windfarm and service boat gives an idea of modern wind turbine which have rotors with blade diameter exceeding 150 m.

Fig 1.3 : Offshore wind farm. Photo : Courtesy of Siemens

There are various constraints like installation limitation, cost, weight, fatigue life and clearance between tower and blade tip during operation while looking out for the choice of rotor diameter. From scaling laws, we can understand what are the challenges associated with wind turbines as it indicates that the power that a wind turbine extract varies as square of rotor diameter whereas aerodynamic and gravity based load of wind turbine varies with cubic and fourth power of wind turbine respectively. Rotors have to be designed with complex structures made up of composite fibre materials so as to maximize the aerodynamic performance while limiting the blade mass increase. Fibreglass epoxy and fibreglass polyester are the most commonly used materials in the fabrication of rotors. Some manufacturers are even using expensive materials like glass fibres and carbon fibres with high tensile modulus in order to achieve desired stiffness without increasing the weight of turbine.

For designing bigger and comparatively lighter rotors, we need to focus more on accuracy of designing tools so as to push the limits of materials and their structure. Material updates and geometry can be easily accommodated from previous designs in blade modelling because of rapidly developing technologies and shorter time period between blade generations. 3D finite element analysis is considered to be expensive for most design process and also it doesn't respond well for design exploration and analysis of various data. We can use beam models to effectively predict the behaviour of rotor blades as cross sectional dimensions of rotor blades is very small as compared to their overall length. 3D behaviour of each blade can be modelled using beam elements upto 10^2 to 10^3 degrees of freedom as compared to shell elements which uses 10^5 to 10^6 degree of freedom.

As shown in fig 1.4, we can see the common process which can be used to develop a reduced model of 3D composite structure using beam elements. First thing we need to do is to take an

individual beam section and calculate its various mechanical properties in order to reduce the blade dimensions. The analysis tools which will be used must be able to analyse both thin and thick cross section having anisotropic and isotropic materials which are generally found in blades of wind turbines. Next step is to get the beam elements stiffness matrices using cross sectional properties. Materials and geometry approach are taken along the blade span during modelling approach. Analysis of large non-linear deformations such as local buckling can be used while doing beam analysis.

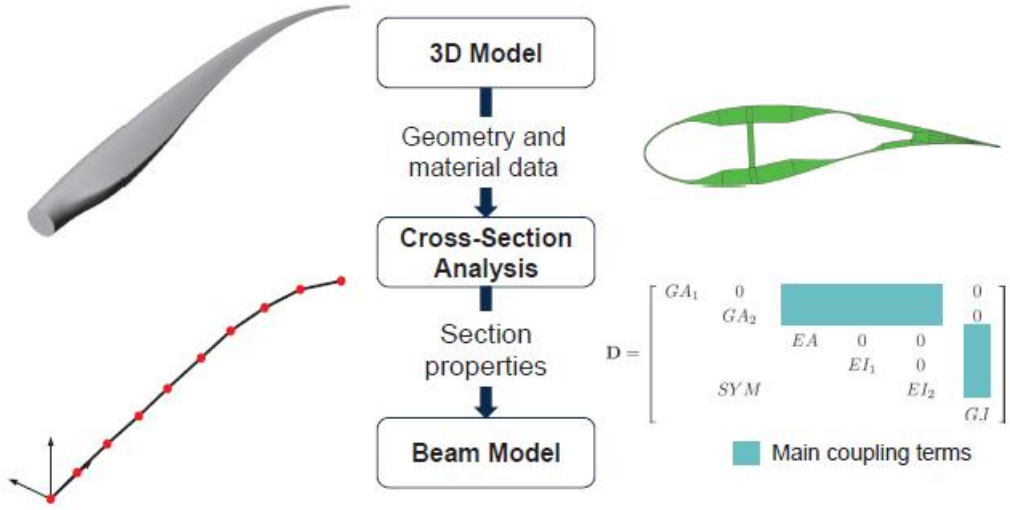

Figure 1.4: Structural blade modelling

1.1 Overview of Large Blade Development Project

Low cost of energy and increase in rotor size has been the consistent trend in commercial grade production of wind turbine all these years. Blade design technology is improved more through optimum material usage and efficient aerodynamic and structural design. Issues related with large wind turbine rotors and blades such as manufacturing, design and materials issues are evaluated by WINDPACT studies which resulted in design specifications of candidate blades ranging from 30 to 70 metres in length [5,6] and rotors ranging from 80 to 120 meters in diameter [6,7]. Further advancement in design for even more larger machines can push the

limit further which is mainly restricted by limitations of weight growth. The objective of the work presented here is to examine the effects of scaling on structural characteristics using CFD analysis tool. Various new innovations in this sector already found includes improved design, materials and manufacturing approach.

1.2 Large Turbines

Maximum length of the blade found in the largest machines in the world was 61.5 meters when this research was beginning. largest available machines from various turbine manufacturers are listed (web survey conducted on January 25, 2011). These machines include rotor diameters upto 128 m with ratings ranging from 2.5 to 6.15 MW. The survey list information which are readily available for use of the public. There are plans going on to develop even more larger machines to produce more energy for better utilization. For example, Clipper Britannia project has proposed to design a machine rated at 10 MW. Studies of other large blades includes work of Hillmer in 2007[8], wherein authors were exploring the possibility of increasing the blade length upto 82 meters.

1.3 Existing Models

Realistic structural models are required in order to perform structural analysis to evaluate designs. Technical data provided by manufacturers are scarce. Independent public studies in past are the only source to get structural model properties from studies of large turbines such as the DOWEC (Dutch offshore wind energy convertor) study [9,10], the UpWind project [11] and the DOE/NREL work [12]. In these studies, blade length ranges from 61.5 to 64.5 meters and turbine ratings varies 5-6 MW.

1.3.1 Study of DOWEC Blade

Study of DOWEC blade [9.10] which includes the development of 64.5 metres blade was carried out during the period of 197-2003. Distributed geometric properties as well as

distributed stiffness and blade mass properties are also presented in this blade research study with other results. Data available from the 64.5 metres blade development study of DOWEC study [9,10] are utilized by both Upwind project [11] and NREL 5 MW model [12].

1.3.2 NREL 5 MW Model

NREL developed an aeroelastic model of 5 MW wind turbine by utilizing the existing conceptual designs of similar size [12]. FAST aero elastic code [13] was used to analyse the 5 MW Model. NREL 5 MW model has been made public and widely available for researchers for their research studies. Models for the nacelle and drive train dynamics are included in this turbine model. It also contains distributed properties for the turbine blades and the tower. Controllers in addition to standard controllers were developed for this turbine model which includes variable speed, yaw and collective control pitch characteristics. Aerodynamics and structural properties of DOWEC study were used by this turbine model for developing its blades, even though the blades were decreased to 61.5 metres from original 64.5 metres.

1.3.3 UpWind 5 MW Model

This is a research program with major concentration on large turbine blades. During this study, 61.5 metre blade design made up of all glass in developed by UpWind researchers similar to the external geometry of DOWEC 64.5 metre blade. Lay-up data of DOWEC blade study was not made publicly available due to its propriety nature. Therefore, an independent material layup was developed by UpWind researchers [14].

1.4 Thesis Layout

This thesis is divided into four major chapters. Literature review is presented from various scholarly publications in 2nd chapter. Detailed discussions with conceptual descriptions are presented here. The information presented here develops a strong foundation for understanding various ongoing methods of studying wind turbines and their scaling effects. Research

Methodology is explained in 3rd chapter. Geometry of wind turbine blade is developed in solid works and is imported to Ansys for simulation of turbine blade at various wind speed conditions for determining characteristics. In 4th chapter, results for structural characteristics is presented for various wind speed and graphs are plotted between them for better understanding. Finally, in 5th chapter, conclusion is drawn from results and future work is predicted for the same.

Chapter - 2

LITERATURE REVIEW

2.1 Scaling Laws for Blade Structural Properties and Design Trends

Scaling laws can be used to extrapolate existing model properties to larger turbine sizes and predict the effect of blade length on design trends such as root bending moments and natural frequencies. In this section we consider general scaling trends.

2.2 Scaling Laws and rules of similarity

Conventional scaling of turbine and blade properties is accomplished by a dimensional analysis, whereby all length dependent variables are scaled according to a scale factor. The theory of similarity is a very simple but powerful theory to investigate the wind turbine scaling effects on its different characteristics. Using this theory, the flow condition is the same in both large and small cases if the following criteria are met [15]

a. The tip speed ratio is maintained in both cases.

b. The blade profile and the number of blades are kept the same.

c. Proportional adjustments are made to all dimensions containing radius, profile chord, and spar size.

In this situation, the triangles of velocity and the relative velocity angles at every related blade cross-section is the same for large and small wind turbines; therefore, flow condition would be the same for the two cases.

Based on these considerations, the effects of the scaling on the performance characteristics of the rotor, forces at the blade, stress at the blade root, and dynamic characteristics can be determined. In the present paper the impact of scaling on structural parameters are examined. These parameters are presented in Table 2.1.

Table 2.1 The relativity of structural parameters to wind turbine rotor diameter.

Parameter	Relativity to rotor diameter
Blade Mass	$\frac{m_2}{m_1} = \left(\frac{D_2}{D_1}\right)^3$
Stresses	$\frac{\sigma_2}{\sigma_1} = \left(\frac{D_2}{D_1}\right)^2$
Force Reaction	$\frac{F_2}{F_1} = \left(\frac{D_2}{D_1}\right)^2$

In these equations, parameter "D" indicates wind turbine rotor diameter (twice the distance of rotor centre to blade tip). The results obtained by CFD simulation will be compared to predictions of the theory of similarity. In addition to parameters introduced in Table 2.1, the number of grid elements in simulation and as a result the computational time dependency on scale of the turbine is of interest.

Scaling laws, based on this dimensional analysis, can be developed for turbine power, blade mass and stiffness properties, root bending moments and other turbine mass properties. In addition to geometric similarity, material similarity and constant tip speed ratio are assumed for this conventional up-scaling.

First, we define a scale factor, α, as the ratio of the scaled blade length (L_U) to the nominal blade length (L_B):

$$\alpha = \frac{Scaled\ Length}{Nominal\ Length} = \frac{L_U}{L_B} \qquad (2.1)$$

where, “U” refers to the up-scaled blade and “B” refers the nominal blade. Alternatively, the scale factor can be defined as the ratio of the scaled rotor radius to the nominal rotor radius "U ".

The total blade mass follows this relationship:

$$m_u = \alpha^3 m_b \qquad (2.2)$$

and the rotor power:

$$P_u = \alpha^2 P_b \qquad (2.3)$$

We immediately observe the well-known fact that as blade length increases blade mass grows at a faster rate (α^3) than rotor power (α^2). Innovations can be utilized to reduce the rate of mass growth. Equation (2.2) is the result of volume scaling because the material density is held constant due to assumed material similarity. Rotor power depends on the swept area of the rotor, thus the squared relationship in Equation (2.3).

Further, the CG location, z, of the blade (or any span-wise location on the blade for that matter) follows the following scaling law:

$$z_u = \alpha^1 z_b \qquad (2.4)$$

Scaling laws can also be developed for the blade response to loads. For example, root bending moments, which are important design drivers, can be written with scaling laws. Expressions for the root bending moments that result from aerodynamic forces or gravitational loads are given below (Eqns. 2.7,2.8). The aerodynamic lift and drag forces can be written as [16]:

$$F_L = \frac{1}{2}\rho A C_L V^2 \qquad (2.5)$$

$$F_D = \frac{1}{2}\rho A C_D V^2 \qquad (2.6)$$

Where ρ is air density, A is area, C_L and C_D are aerodynamic coefficients, and V is velocity. Both expressions for the aerodynamic force have the same mathematical form. The velocity depends on the inflow wind speed as well as the rotational rate. When assuming constant tip speed ratio for up-scaling, the velocity field along the blade is a constant. In order to maintain constant tip speed for longer blades, the turbine operating speed is reduced linearly. Area, then, is the only variable dependent on scale in these equations, thus aerodynamic forces, both lift and drag, scale with the square of the scale factor.

We now consider bending moments due to aerodynamic loads. The bending moments arise from the product of force on the blade elements (an α^2 dependence) and the span-wise location of the applied load (an α^1 dependence). Thus, moments due to aerodynamic loads are scaled by the following cubic relation:

$$M_u^{Aero} = \alpha^3 M_B^{Aero} \qquad (2.7)$$

We now consider root bending moments due to gravitational loads. These moments arise from the product of blade weight and its span-wise location. For conventional up-scaling, blade mass grows as the cube of the scale factor (See Equation 2) while location scales linearly. Therefore, moments due to gravitational loads grow with the fourth power of the scale factor:

$$M_u^{Gravity} = \alpha^4 M_u^{Gravity} \qquad (2.8)$$

Thus, we can see from Equations 2.7 and 2.8 that moments due to gravitational loads scale at a faster rate than aerodynamic loads. For blades on today's machines, aerodynamic loads are typically larger than gravitational loads. Thus, root bending moments due to aerodynamic loads have been a principal design driver especially in the flap-wise direction. However, it is clear that as blade length increases, root bending moments due to gravitational loads will grow to exceed moments due to aerodynamic loads. Gravity loads are primarily resisted in the lead-lag direction. Much larger gravity loading will require additional reinforcement and design

adjustments in the lead-lag direction and beefed up components all the way through the turbine system itself.

The root bending moment relations can be re-written in terms of stress or strain. One finds that stress (and strain) due to aerodynamic loads is independent of scale (α^0). On the other hand, stress (and strain) due to gravitational loads grow linearly (α^1) with scale. Observing these trends is important for strength and fatigue calculations, and demonstrates important design considerations for edge-wise strains.

The natural frequencies of blade bending modes drop linearly with the scale factor (an α^{-1} dependence). This trend can be observed by considering an analytical formula for the natural frequency of a beam with uniform cross-section:

$$f_i = \frac{{\lambda_i}^2}{2\pi L^2}\sqrt{\frac{EI}{\rho A}} \qquad (2.9)$$

where λ_i is a constant associated with the i^{th} mode, L is the beam length, E is Young's Modulus, I is the area moment of inertia, ρ is density, and A is cross-sectional area.

With material similarity, E and ρ, are held constant while only the geometric variables are scaled. The result is

$$f_i^u = \frac{1}{\alpha}\frac{{\lambda_i}^2}{2\pi L^2}\sqrt{\frac{EI}{\rho A}} \qquad (2.10)$$

$$= \frac{1}{\alpha} f_i$$

However, on a per rev basis natural frequencies (natural frequency divided by the operating speed) are independent of scale because the operating speed also scales as α^{-1}.

2.3 THEORETICAL UPSCALING

The first approach that has been followed for determining the characteristics of the proposed large wind turbines was based on standard, self-similar geometric upscaling, assuming geometric and aerodynamic similarity (fixed tip speed). This pathway provides a first approximation of critical operational and structural properties and helps in identifying possible technical barriers associated with upscaling. If geometrical similarity is enforced, the weight and power, which are the main criteria we are using, scale according to $m \sim s^3$ and $P \sim s^2$, respectively, where s is the scaling factor. In Table 2.2, the main characteristics (rotor diameter, tip speed and hub height) for power outputs from 5 to 20 MW are given, when simple scaling laws are used. The IEA 5 MW wind turbine is used as reference [17] for the 5 MW size.

Scaling in such a way, the aerodynamic forces for any linear scale (denoted by s) follow an s^2 rule (as the area increases in this manner), while the corresponding moments follow a cubic law (s^3). The section bending stiffness (EI) follows an s^4 rule, resulting in scale-invariant bending stresses due to aerodynamic forces (as they follow M . y=EI/. The same applies for tension stresses, with centrifugal forces scaling as $m \cdot \omega^2 \cdot R$, so that, for constant tip speed, the overall force scales following the square law. The cross section will also follow the square law resulting in constant tension stresses. On the other hand, tension/compression and bending loads due to self-weight scale as s^3 and s^4, respectively, resulting in a linear scaling of the corresponding stresses.

In short, neglecting second-order aerodynamic effects and assuming linear structural behaviour, we end up with what we call “classic similarity laws”. A key finding of classic similarity as we described it, is that stresses due to aerodynamics loading appear due to invariant during upscaling, whereas those due to weight are linearly increasing with the geometric scaling factor.

A typical example of a beam-like structure subject to such loadings is a tubular support structure with linearly varying diameter (D) and wall thickness (t). Because of the simple geometry of this component, we will use it to illustrate the results of geometrical upscaling. In this context, upscaling will be considered under the prism of the following combined design loads.

- Tower bending due to rotor thrust
- Tower bending due to wind loads on the tower
- Tower axial and bending loads from weight, including tower self-weight and tower-top components (nacelle and rotor)

The design criterion is buckling under ultimate compression, considering a quasi-steady load condition. The design work is carried out according to the guidelines of DIN 18800 on Structural Steelwork [18]. The maximum normal stress in an arbitrary section (z) of a beam-like structure, subjected to a normal force F and a bending moment M, is given by

$$\sigma_{max} = \frac{F}{A} + \frac{M}{W_m} \rightarrow \sigma_{max}(s) = \frac{F(s)}{A(1) \cdot s^2} + \frac{M(s)}{W_m(1) \cdot s^3} \qquad (2.11)$$

where A(z) is the area of the section and $W_m(z)$ is its resistance in bending. The overall design stress is then calculated from the superposition of the individual maximum normal stresses that correspond to the different load components. ($F_{1,2}$, $M_{3,4,5}$), as $\sigma_{ALL,max} = \Sigma\sigma_{max,i}$. For the case of geometrical upscaling, the result of the superposition is shown in Figure 1, with the calculation performed for the base section. The buckling limit is also shown, calculated according to the guidelines of DIN 18800 on Structural Steelwork. Note that the buckling limit is completely insensitive to scale *only* in the strict case of geometrical upscaling, where its deriving formula—based on non-dimensional geometric properties such as the t/D ratio—is scale independent. It is obvious that, as discussed, stresses due to aerodynamic forces are scale

invariant, whereas stresses due to weight are linearly increasing with the scale factor. As a consequence of this, classical upscaling is not possible beyond a certain s value, as the stress, increasing linearly, will exceed at that point the design stress limit.

Table 2.2. Design parameters and 'base' values

	Power, P (MW)			
	5	10	15	20
Rotor diameter, D (m)	126	178	218	252
Maximum Tip speed, U_t (m s^{-1})	80	80	80	80
Hub height, H (m)	90	116	136	153

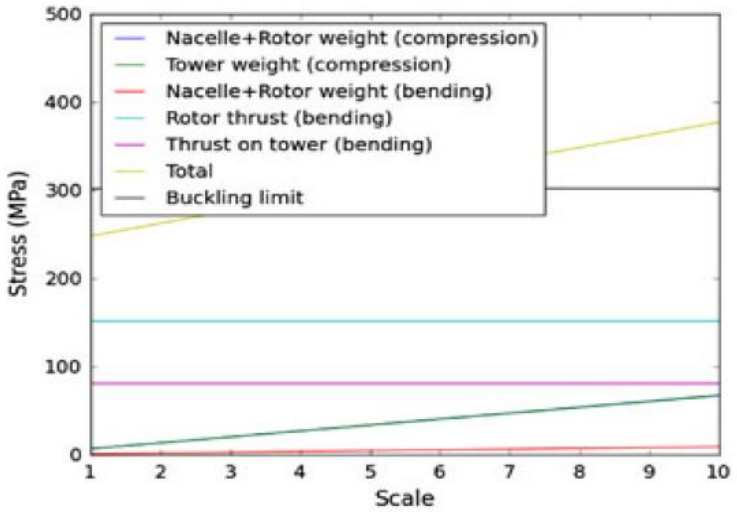

	Top weight (c)	*Tower weight (c)*	*Top weight (b)*	*Rotor thrust (b)*	*Tower thrust (b)*
5MW	2.70%	2.70%	0.40%	61.40%	32.90%
10MW	3.80%	3.70%	0.50%	59.90%	32.10%
20MW	5.10%	5.10%	0.70%	58.00%	31.10%

c=compression, b=bending

Figure 2.1. Stress distribution for different scales from 1 to 10. The percentile contribution of each source to the overall stress is given in the table for different sizes.

The contribution of the various stress components for three turbine sizes (5, 10 and 20 MW) is also shown in Figure 2.1, illustrating the relative magnitude of each stress component, based on the same reference 5 MW wind turbine [17]

The calculation of the various loads is not performed for the same operating point, as the extreme aerodynamic thrust on the rotor (based on rated conditions) and the tower (based on extreme gust conditions) are not fully consistent. Assuming that, for a pitch controlled turbine, the rotor thrust under extreme gust is less or equally severe with the thrust at rated conditions, we apply the above-mentioned combination for simplicity, having also in mind that we are not mainly interested in the exact loads of the reference turbine but in establishing the scaling trends of these loads.

Similar conclusions can be derived for the other parts of the wind turbine. The rotor blades, being cantilevered beams with the design driven by aerodynamic bending moments, will also scale cubically in mass, unless the cyclic weight fatigue loading becomes the design-driving load instead. The scaling rules for the drive train are not as straightforward and depend on its actual configuration. The gearbox input torque will increase cubically, but if a constant output speed is required, the increased gear ratio required will result in a further mass increase. This could be offset by the fact that the constant-speed generator size will then increase following power (s^2). For a direct-drive generator, the situation is simpler and a cubic law is expected (following torque).

A full set of scaling laws for all the components has been developed during this project, including loads, Eigen frequencies, masses, etc., and is reported in detail in Chaviaropoulos [19].

However, these geometric similarity rules are approximations. Some of the effects that have not been included in the 'theoretical' upscaling laws are as follows:

- Boundary layer effects related to the blades—change in the Reynolds number implies change in loads. As the Reynolds number is already large for the reference wind turbine, it is not expected that the effect will be substantial.
- Wind shear effect. The power **P** from a wind turbine rotor of radius **R** in a steady wind field of velocity **V** is proportional to V^3R^2, and assuming geometric similarity, the hub height ***h*** is proportional to **R**. In the presence of wind shear characterized by a wind shear exponent **α**, **V** is proportional to $\mathbf{h}^{\boldsymbol{\alpha}}$. Hence, power becomes proportional to $\mathbf{R}^{\mathbf{2+3\alpha}}$. The bending moment on a blade (**M**) is proportional to $\mathbf{V^2R^3}$, and a similar analysis establishes that it will be proportional to $\mathbf{R}^{\mathbf{3+2\alpha}}$. Hence, both power and loading will be somewhat influenced by the difference in shear expected in large sizes.
- Size effects related to the fracture mechanics of materials—implying an upscaling exponent larger than 3
- Size effects related to increased risk of buckling failure modes by upscaling
- Increased risk by geometric upscaling of low-cycle fatigue failure from weight-induced loads
- Non-linearities due to large deflections (e.g. see Riziotis **et al.** [20] for findings concerning the 5 MW machine considered here).
- Effects of the inflow turbulence on the dynamic behaviour. As the rotor size increases, the spatial coherency of the incoming wind decreases, resulting in lower loads for the rotor and tower, better power quality and lower rotor speed fluctuations. On the other hand, the energy of the wind concentrates mainly on multiples of the rotational frequency that indicates that the wake-induced effects will have a strong variation with the azimuth [21].

- Changes in design choices, especially for offshore applications where the technology is still evolving and different configurations are being considered for both fixed-bottom and floating structures. These can result in large variations in the structure weight that are not a direct result of the scaling.

It is these shortcomings of the simplified method that led to the next step, where the actual upscaling trends of wind turbines are studied.

2.4 REAL UPSCALING

Purely geometrical upscaling offers useful insight but fails to cover all aspects of the operation of large size wind turbines. In order to quantify the actual upscaling process that has been used in wind turbine design and manufacturing, we employ a different method, based on the study of observed industrial trends. The main questions that need to be answered by such a study are as follows:

- How do actual loads scale in real wind turbine designs?
- What is the weight increase law for upscaling?
- What is the cost increase law for upscaling?

In order to answer the first question, we use the load calculations that have been performed by GH (Garrad Hassan) for wind turbine manufacturers as a typical set [22]. These calculations are typically performed in conformance with GL or IEC standards [23]. Because of design configuration differences and the influence of wind class, the load cases that create design-driving extreme or fatigue loads vary considerably. Nevertheless, such data can be viewed collectively to see what information can be derived in terms of scaling trends. While the disadvantage of this data source is in the diversity of designs and external design conditions considered, a major advantage is that the data are totally ‘real world’ and in no way simplistic, with loads derived by rigorous calculation procedures, approved by certification

bodies and used by manufacturers in the design of their turbines. Only pitch regulated wind turbines have been considered for this study, and trend lines for the various examined loads have been derived. All kinds of extreme and fatigue loads have been examined, and typical results (for moments at the tower base and at the blade root) are shown in Figure 2.2 (the load component names conform to the GL coordinate system). In scaling with similarity, moments would follow a cubic law or greater where self-weight loading is involved. Each of the curves of Figure 2.2 are based on approximately 50 data points from detailed load calculations performed to certification standards. A wide variety of turbine design styles (concepts and operational characteristics) and design site conditions (IEC Class 1, Class 2 and others) are grouped together. This limits the statistical significance in determination of characteristic exponents, although some variations are striking and appear to be consistent.

The high scaling exponent of tower base M_z (yaw moment) is interesting (the same happens for the tower top that is not shown). The yaw torque arises as a consequence of differential blade loading. It may be that the effect of turbulence in creating differential loading across the rotor disc, which is becoming more severe at large scale, is being registered here. Fatigue load exponents also tend to exceed simple cubic scaling, given that above rated wind speed, when most fatigue damage is accumulated; the blade self-weight will introduce cyclic loading in both the M_x and M_y (fore-aft and side) components (the effect will be even greater for the blades' loading). An increasing effect of turbulence with scale may also be contributory to the exponents' being greater than cubic. On the other hand, the reduction in RPM, due to the constant tip speed assumption, will reduce the fatigue loading.

A similar procedure was used to answer the second question and estimate the weight of the main components, based on actual parts instead of upscaling theory. The diameter of the wind turbine was used to indicate the scale (rated power could also be used, but a geometrical quantity was deemed preferable). Results for nacelle and blade masses are given in Figure 2.3.

Interestingly, both seem to scale with exponents well below the cubic law that the similarity laws dictates. In the case of the nacelle weight in particular, weight seems to follow an s^2 law, indicating an almost constant power/weight ratio. For the blades, the last three points shown in the figure correspond to projections for blades larger than ones presently available, assuming that the current trend continues.

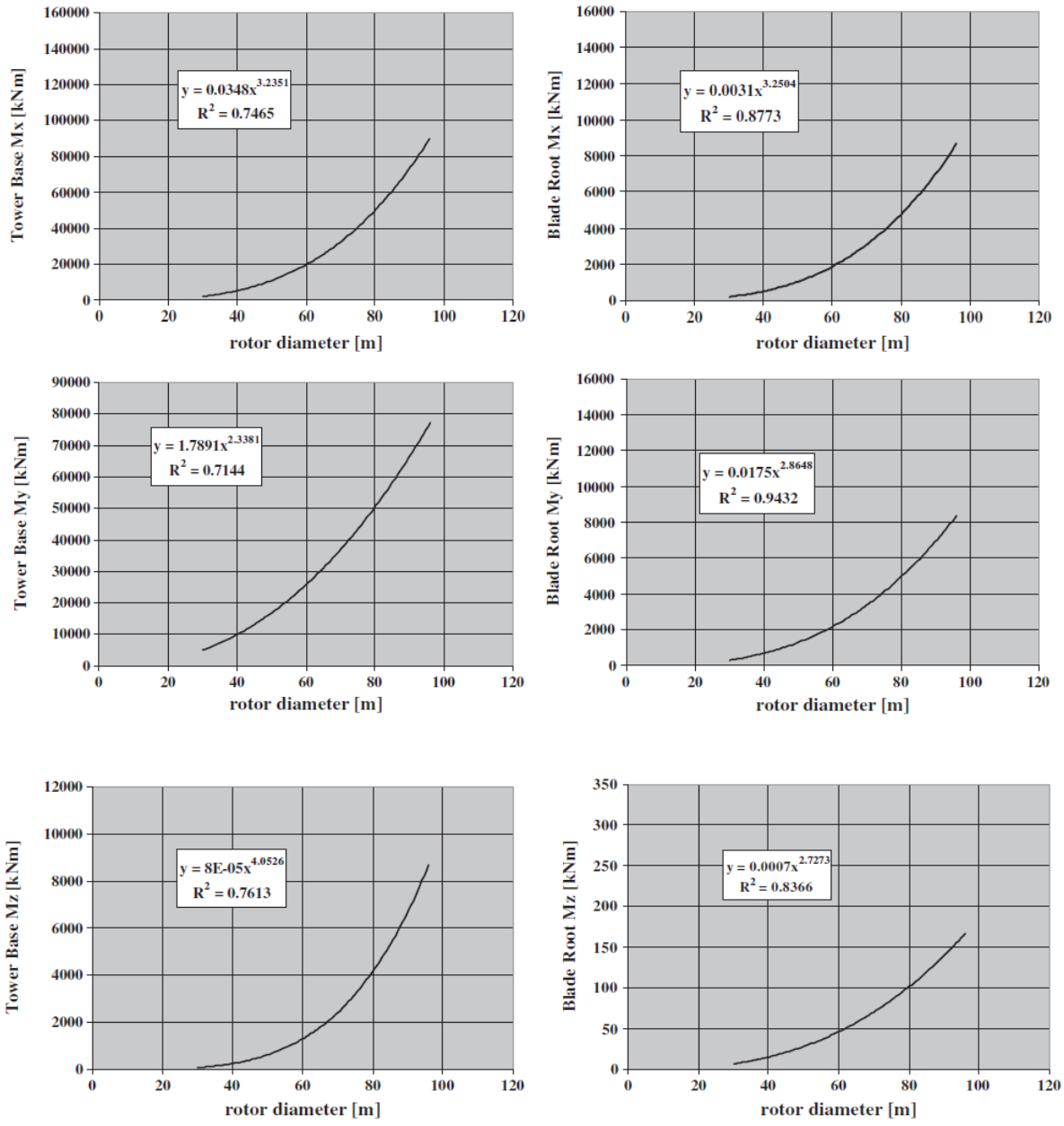

Figure 2.2. Design extreme loads based on real data. Tower base (left) and blade root (right) moments

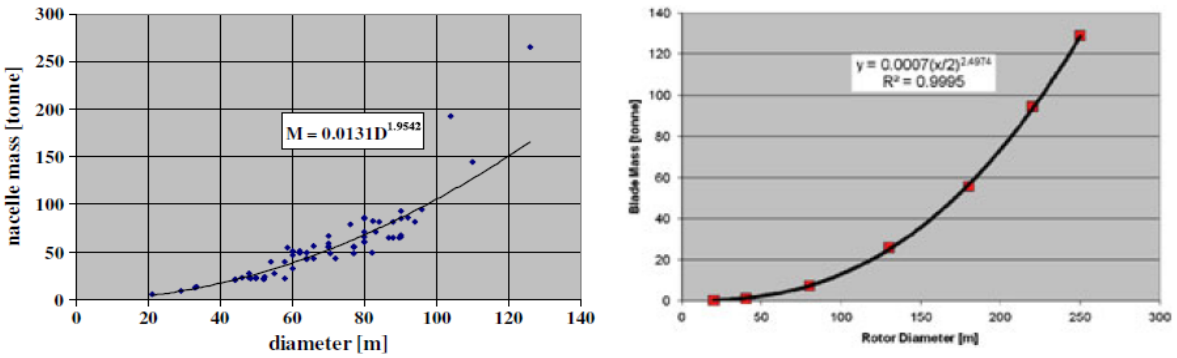

Figure 2.3. Mass as a function of size for nacelle and blades

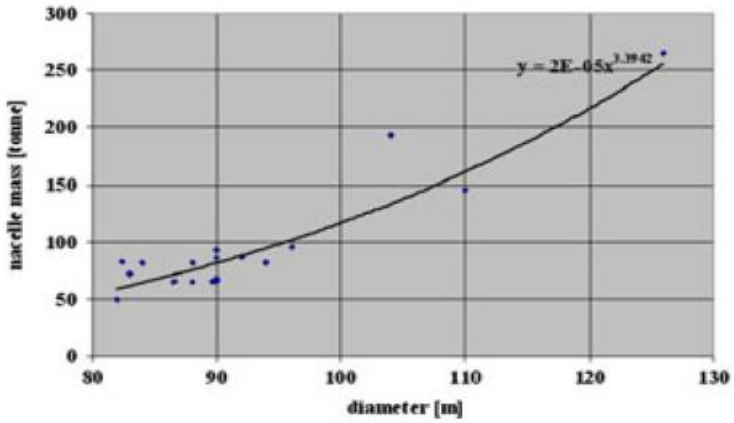

Figure 2.4. Mass as a function of size for nacelle considering only large size wind turbines

Unfortunately, the method used for the weight estimation introduces a bias that can distort the trend lines and lead to erroneous conclusions. The dataset used includes small wind turbines of relatively old design and (fewer) large wind turbines, all of which are of relatively recent design. It is therefore difficult to differentiate between the effects of upscaling and those of the technology improvements that came with the larger machines. If the same regression is performed for the nacelle weight, keeping only recent wind turbines with rotor diameter D

> 80 m, a different picture emerges, as seen in Figure 2.4, with the scaling exponent increasing, in closer agreement to the upscaling theory. An indication of the bias introduced by technology evolution is better seen when the weight increase of blades is considered, as the technology 'steps' associated with blade materials are well defined historically [24]. The size correlations for each technology (glass epoxy, hybrid, etc.) are closer to the theoretical predictions, as seen in Figure 2.5. The first three curves and corresponding scatter points representing existing technologies (with hybrid having the lowest weight), whereas the last two give a projection of future technology, if the current trends continue.

In order to have a physical insight of the scaling process, independently of the technology level, we use the same simplified tower problem that was described earlier. Instead of geometrical upscaling, we require constant-stress upscaling, introducing the scaling functions $\mathbf{g_D\,(s)}$ and $\mathbf{g_t\,(s)}$, which quantify the departure from geometrical upscaling in diameter and thickness, respectively. The objective of the optimization problem is to minimize the product $\mathbf{g_D\,(s)\,.\,g_t\,(s)}$ (which is equivalent to minimizing the weight for each scale) while constraining the overall stress below its design limit (for local buckling in this case). Using a constrained optimization algorithm [25], with $\mathbf{g_D}$ and $\mathbf{g_t}$ as the optimization variables, the resulting $\mathbf{g_D\,(s)\,.\,g_t(s)\,s}$ distribution, representing the extra weight needed in comparison to classical upscaling, is shown in Figure 2.6(a) (the optimization is performed independently for different scales). It is also seen that this extra weight term is always greater or equal ($\mathbf{s = 1}$) to 1 and almost linearly (in this particular case) increasing with scale. Intuitively, one would expect, since $\mathbf{g_D\,(s)\,.\,g_t\,(s)} \geq \mathbf{1}$, that increasing the scale, the weight forces are increasing accordingly, and more material is then needed for resisting the elevated stress level.

The corresponding overall weight represented by the non-dimensional volume $\mathbf{s^3.\,g_D\,(s)\,.\,g_t\,(s)}$ versus $\mathbf{s}$ is shown in Figure 2.6(b) in a log–log plot. Assuming that weight scales up following an $\mathbf{s^x}$ law, we calculated the mean exponent ($\mathbf{x}$) for this expression through a best-fit procedure.

This is evidently resulting in an $\mathbf{x = 3^+}$ exponent, as expected based on the previous discussion. It should be pointed out that the actual weight does not really scale following $\mathbf{s^x}$ (the extra weight is nearly linear with the scale). The false impression that an exponential representation of weight scaling is representative comes from the fact that the deviation of **x** from its prevailing component 3 is rather small. We shall nevertheless continue to use this representation to provide estimates of the deviations from geometrical similarity.

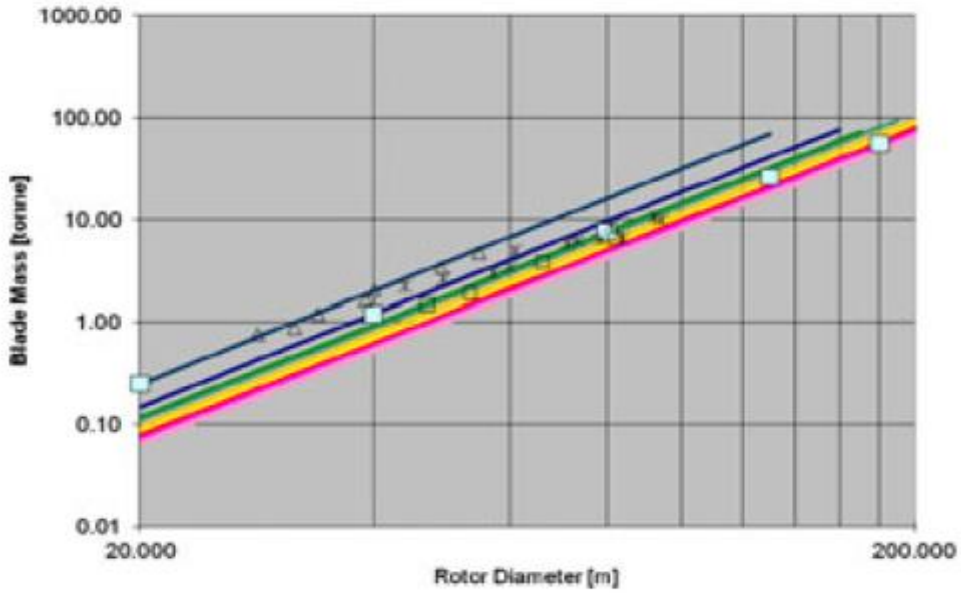

Figure 2.5. Blade mass as a function of size for different technologies (filled squares denote the combined size and technology improvement trend)

A strict proof that $\mathbf{g_D(s) \cdot g_t(s) \geq 1}$ always holds, suggesting that we cannot upscale beam-like structures with a weight exponent less than 3, can be given. In order to do that, we further assume that the **t/D** ratio remains constant in upscaling (equivalent to setting $g_D(s) = g_t(s)$), thus eliminating one degree of freedom from the optimization procedure. The validity of the assumption is tested by comparing the results of Figure 2.6 (two degrees of freedom, D and t) against those of Figure 2.7 (one degree of freedom, D).

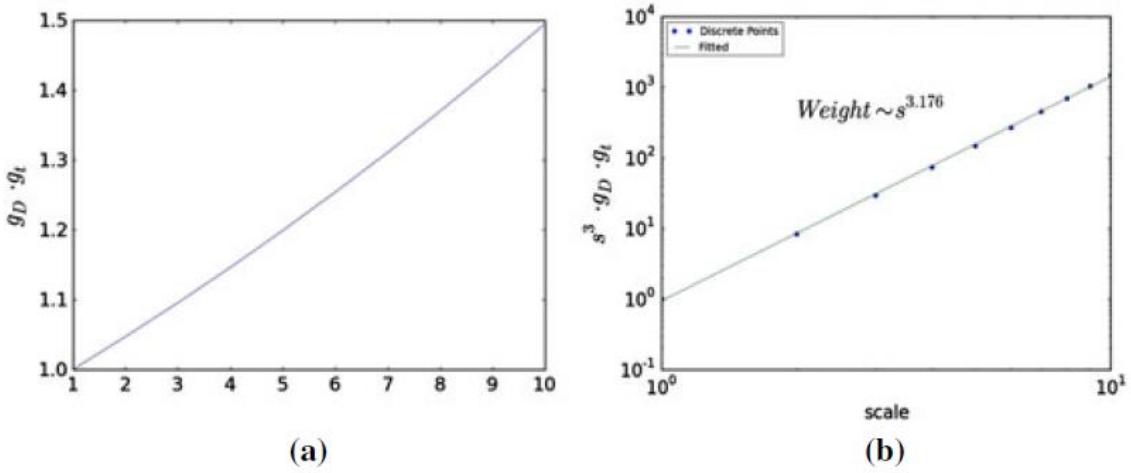

Figure 2.6. Scaling functions (a) and weight (b) increase with scale for a simplified tower structure

In this case, thickness and diameter scale in the same way, as D(s) = D (1) . s . f(s), and t(s) = t (1) . s . f(s), where f (s) is a function of the scale with f(1) = 1. The area of a given section will then scale as A(s) = A(1) . s^2 . $f^{2(}$s) and the mass as m(s) = m(1) . s^3 . f^2 (s).

Following above, the overall maximum stress reads

$$\sigma_{ALL,max}(s) = \frac{\alpha_1 \cdot s}{f^2\ (s)} + \alpha_2 \cdot s + \frac{\alpha_3 \cdot s}{f^3\ (s)} + \frac{\alpha_4 \cdot 1}{f^3\ (s)} + \frac{\alpha_5 \cdot 1}{f^2\ (s)} \qquad (2.12)$$

where the constants $\alpha_1,\ldots,\alpha_5$ are expressed in terms of geometrical and load data of the reference (s = 1) turbine and represent the actual stress from each of the five load mechanisms considered (compression from top-weight, compression from tower weight, bending from top-weight offset, bending from rotor thrust and bending from thrust of air on the tower; in this order, details are in Sieros and Chaviaropoulos[26]). The last two terms, which do not have a direct dependence on scale, represent by far the largest contribution in small scales.

Introducing the non-dimensional coefficients $b_i = \alpha_i / \sigma_{ALL,max}(1)$, we come to the following equation that the unknown function f (s) must satisfy for every value of s:

$$\frac{b_1 \cdot s}{f^2\ (s)} + b_2 \cdot s + \frac{b_3 \cdot s}{f^3\ (s)} + \frac{b_4 \cdot 1}{f^3\ (s)} + \frac{b_5 \cdot 1}{f^2\ (s)} = 1 \qquad (2.13)$$

Note that, according to their defining relation, $b_{1,\ldots,}b_5$ express the ratio of the corresponding load component to the design stress limit of the reference wind turbine. For the given (b_i, s), equation (3) can be solved for f (s). The previous equation can be written in the general form

$$G(f) = f^3 - af - b = 0 \qquad (2.14)$$

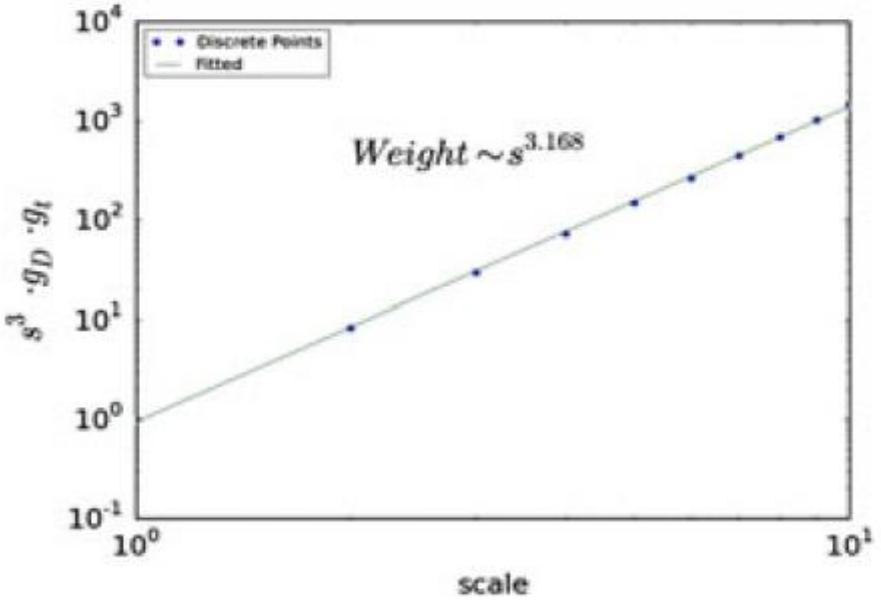

Figure 2.7. Weight increase with scale-simplified model ($g_D = g_S$)

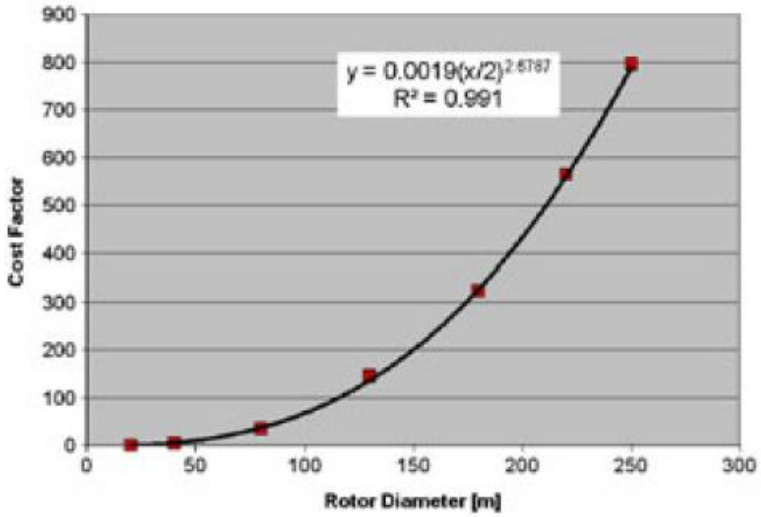

Figure 2.8. Blade cost as a function of scale

The behaviour of G(f) can be analysed based on its roots, and there is always one real positive solution, which is larger than 1 when a+b > 1 and smaller than 1 when a+b < 1. The above analysis shows that there is always one single positive solution of for equation (4) for f(s), with f (1) = 1 and f (s)>1 for any s > 1. That means that it is not possible to upscale without having a weight increase of $\geq s^3$. More details regarding this constant-stress upscaling problem can be found in Sieros and Chaviaropoulos. [26,27]

Note that the above conclusions have been derived taking account of normal stresses only and assuming that the limiting factor will always be the buckling limit. However, as long as the combined loading can be expressed as a combination of terms like the above, the conclusions will not differ greatly for other types of loading and components, although the relative magnitude of the terms will differ (e.g. weight-induced cyclic loading will have a bigger contribution in blade fatigue calculations).

The final question about upscaling concerns the cost increase associated with size. Previous studies [28] indicate that weight is the major driver for component cost, but the two do not

scale in exactly the same way. For this reason, a study similar to the one for weight was performed for the cost of typical wind turbine components. Results for wind turbine blades are shown in Figure 2.8. Similar results can be obtained for other components, but as the variation in configurations is greater, it is harder to derive concrete conclusions.

2.5 Blade element momentum theory

The steady state aerodynamics of wind turbines is commonly analysed by using momentum and blade element theory. Momentum theory refers to a control volume analysis of the forces acting on the blade based on the conservation of linear and angular momentum. Blade element theory refers to an analysis of forces at a blade section, as a function of blade geometry. According to the blade element theory, the forces on the blades of a wind turbine are expressed as a function of lift and drag coefficients and the angle of attack (AoA). The results of these approaches can be combined into what is known as strip theory or BEM theory.

The BEM theory is based on the subdivision of the rotor disk into concentric rings of radial width dr and mean radius r. Each ring intersects the rotor blades forming blade elements or strips. The flow data and the aerodynamic forces acting on each strip are determined by solving two equations, obtained by combining linear and angular momentum conservation and classic lift and drag theory. One equation results from equating the ring axial thrust determined with the one-dimensional (1D) conservation of the linear momentum to the axial thrust computed with the lift and drag forces acting on the blade strips intersected by the ring. The other equation results from equating the ring torque determined with the 1D conservation of the angular momentum to the torque produced by the lift and drag forces acting on the intersected strips. The main geometric and aerodynamic parameters of a generic strip is depicted in Fig. 2.9, in which the section lift and drag forces are denoted by dF_L and dF_D respectively. Denoting by dT

the thrust acting on a ring, the local thrust coefficient is $C_T = dT/(0.5\rho U^2 dA)$, where $dA = 2\pi r dr$ is the area of the ring, and ρ and U are the freestream density and velocity respectively. The local thrust coefficient computed using the conservation of linear momentum is:

$$C_T = 4a(1-a) \qquad (2.15)$$

where a is the axial induction factor. The local thrust coefficient computed using lift and drag theory is:

$$C_T = \frac{\sigma_r.(1-a)^2}{sin^2\,\varphi}(C_L \text{Cos } \varphi + C_D \text{Sin } \varphi) \qquad (2.16)$$

where $\sigma_r = (N_b c)/(2\pi r)$ is the local solidity, N_b is the number of blades, c is the airfoil chord length, and C_L and C_D are the lift and drag coefficients respectively. The symbol φ denotes the angle of the relative wind velocity vector U_{rel} on the rotor plane. Its expression is $\varphi = \arctan[(1-a)/((1+a')\lambda_r)]$, where a′ is the circumferential induction factor and $\lambda_r = \Omega r/U$ is the local speed ratio, where Ω is the angular speed of the rotor. U_{rel} is expressed as $U_{rel}=U(1-a)/\sin\varphi$. Equating Eqns. 2.15 and 2.16 yields one equation in the two unknowns a and a′, since C_L and C_D are ultimately also functions of the induction factors.

In fact, these force coefficients can be obtained with panel or CFD codes (see Sect. 2.2 for details) or experimental data as functions of the Reynolds number (Re), which depends on U_{rel} and the relative AoA α, the angle between the air foil chord and U_{rel}. As shown in Fig. 2.9, $\alpha = \varphi - \theta p$, where θp is the section pitch angle. This parameter depends only on geometric features, and its expression is $\theta p = \theta_{p,0} + \theta_T$, where $\theta_{p,0}$ is the pitch angle of the blade and θ_T is the section twist angle. Denoting by dQ the torque acting on a rotor ring, the local torque coefficient is $C_Q = dQ/(0.5\rho U^2 r dA)$. The local torque coefficient computed using the conservation of angular momentum is:

$$C_Q = 4a'(1-a)\lambda_r \qquad (2.17)$$

The local torque coefficient computed using lift and drag theory is:

$$C_Q = \frac{\sigma_r.(1-a)^2}{sin^2\,\varphi}\,(C_L \,Sin\,\varphi - C_D\,Cos\,\varphi) \qquad (2.18)$$

Equating Eqs. 2.17 and 2.18 yields another equation in the two unknowns a and a′. The nonlinear system resulting by equating the two expressions of C_T and C_Q for each strip need to be solved with an iterative routine based for instance on Newton's method or the method of successive substitution. The two-dimensional (2D) C_L and C_D data are stored in tables as functions of Re and α, and such data are computed in a pre-processing step. Once the flow state of each strip is known, the elemental power dP can be computed. The non-dimensional local power coefficient $C_P = dP/(0.5\rho U^3 dA)$ can be expressed as follows:

$$C_p = \frac{\sigma_r.(1-a)^2\lambda_r}{sin^2\,\varphi}\,(C_L \,Sin\,\varphi - C_D\,Cos\,\varphi) \qquad (2.19)$$

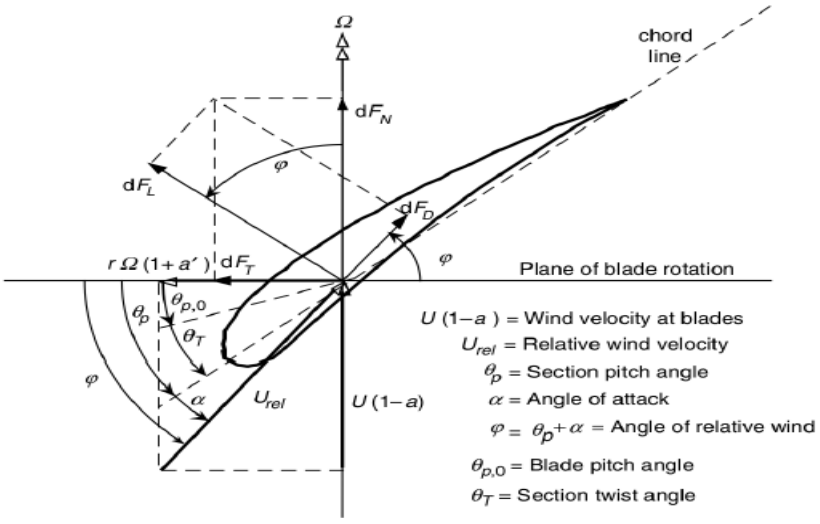

Fig. 2.9 Geometric and aerodynamic parameters of a generic blade strip. Image reproduced from [29].

The mechanical power of a given rotor corresponding to a particular value of U and Ω is determined by integrating dP from the blade root to its tip.

2.5.1 BEM theory corrections

Due to its simplicity, the BEM theory has several limitations. First of all, BEM calculations are static. This assumes that the flow field around the airfoils is always in equilibrium, and the flow accelerates instantaneously to adjust to new inflow or turbine operating conditions. In practice, however, the time taken by the flow-field to reach a steady-state can be relatively long, and, as explained below, the unsteady aerodynamic effects can play an important role in defining wind turbine operating conditions. Alternative methods based on the generalized dynamic wake model [30] have been used to overcome this limitation. Another limitation is tied to the fact that the BEM theory assumes that momentum is balanced in a plane parallel to the rotor. In the presence of large blade deflections this assumption will lead to inaccurate aerodynamic predictions. Moreover, BEM theory assumes the forces acting on the blade are essentially 2D, neglecting the complex 3D phenomena occurring over the rotating blades. As discussed in Sect. 2.2, this limitation is circumvented by means of corrections directly applied on the static force coefficients of the airfoils. Other limitations, described below, come from the inability of BEM theory to model tip and hub losses, flows characterized by high induction factors, and skewed inflow.

2.5.2 Tip and hub loss correction.

As shown in Fig. 2.10, helical vortices are shed from the blade tips into the wake. Tip vortices play an important role in defining the induced velocity field around the rotor. The most common approach to include tip loss in the BEM theory is

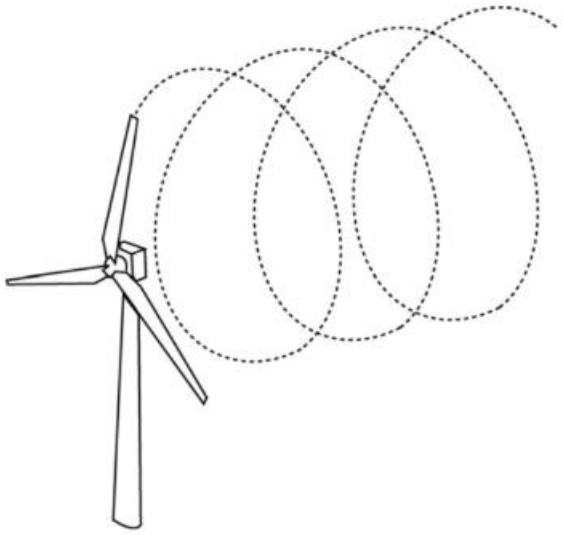

Fig. 2.10 Tip vortex pattern. Image reproduced from [31].

the one developed by Prandtl [29]. This method accounts for tip loss by means of a correction factor F_{tip} defined as follows:

$$F_{tip} = \left(\frac{2}{\pi}\right)\arccos\left(exp\left[-\left\{\frac{N_b(R-r)}{2r\sin\varphi}\right\}\right]\right) \qquad (2.20)$$

where R is the tip radius. When the tip correction is used, Ftip increases as the radial position approaches the blade tip, ranging from zero near the root to unity at the tip. To account for the vortices being shed at the blade hub, a correction for hub loss was developed. This correction is based on a correction factor F_{hub} expressed as:

$$F_{hub} = \left(\frac{2}{\pi}\right)\arccos\left(exp\left[-\left\{\frac{N_b(r-R_{hub})}{2R_{hub}\,Sin\,\varphi}\right\}\right]\right) \qquad (2.21)$$

where R_{hub} is the hub radius. The combined effect of tip and hub losses is taken into account by means of the Prandtl's correction factor F_{Pr} defined as:

$$F_{Pr} = F_{tip}\, F_{hub} \qquad (2.22)$$

F_{Pr} is used to modify the momentum part of the BEM theory, replacing Eqns. 2.15 and 2.17 with the following ones:

$$C_T = 4F_{Pr}a(1-a) \qquad (2.23)$$

$$C_Q = 4F_{Pr}a'(1-a)\,\lambda_r \qquad (2.24)$$

2.5.3 Glauert correction.

During normal operation, wind turbines typically work in the windmill state, in which the axial induction factor ranges from 0 to 0.5. When wind turbines operate at higher tip-speed ratios1 (for example during start up or shut down), the rotor enters in the so-called turbulent wake state [29], in which the axial induction factor is greater than 0.5. For axial induction factors greater than 0.5, BEM theory is no longer valid as, according to momentum theory, this operating state results when some of the flow in the far wake starts to propagate upstream. Flow reversal is not physically possible, and what actually happens is that the flow patterns through the wind turbine become much more complex than those predicted by momentum theory. Above an axial induction factor of 0.5, measured data indicate that thrust coefficient increases up to about 2 at an axial induction factor of 1. To compensate for this limitation Glauert [32] developed a correction to the rotor thrust coefficient based on experimental measurements. As shown in Fig. 2.11, in the windmill state, for axial induction factors up to 0.4, the mathematical relation between C_T and a is expressed by the classical momentum equation. For axial induction factors greater than 0.4, the Glauert correction takes over, intersecting tangentially the classical momentum curve. A numerical problem arises when the Prandtl's correction factor F_{Pr} is included in the classical momentum theory, as shown in Eq. 2.23. In this case, the application of the classical Glauert formulation leads to a gap between the classical momentum curve and the empirical one. In practice, the classical momentum curve and the Glauert curve do not

intersect each other anymore. This gap creates a numerical discontinuity when a computer is used to iterate for the induction factor. To deal with this problem, Buhl [33] derived a modification of the

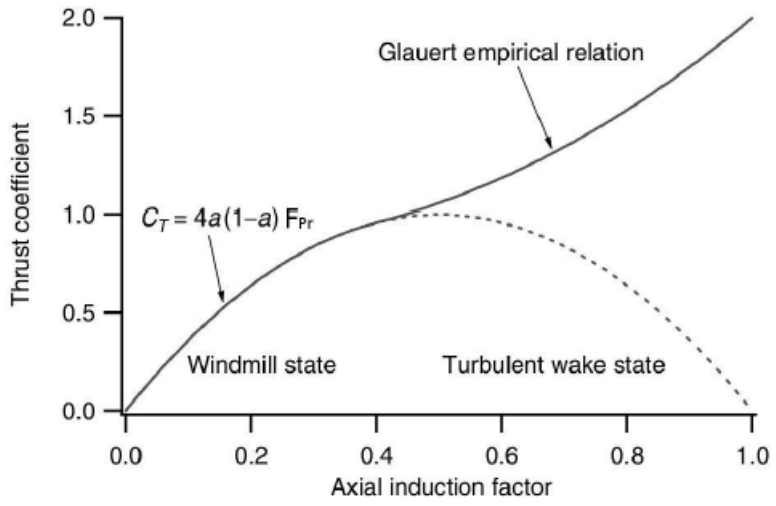

Fig. 2.11 Thrust coefficient versus axial induction factor. Image reproduced from [42].

Glauert correction including the Prandtl's correction factor as follows:

$$\mathbf{C_T} = \frac{8}{9} + \left(4F_{pr} - \frac{40}{9}\right)\mathbf{a} + \left(\frac{50}{9} - 4F_{pr}\right)\mathbf{a^2} \qquad \textbf{(2.25)}$$

Taking into account the value of F_{Pr} explicitly, Eq. 2.25 always guarantees continuity between the classical momentum curve and the Glauert one.

2.5.4 Skewed wake correction.

Wind turbines often operate with a non-zero yaw angle relative to the wind inflow. This determines a skewed wake behind the rotor. BEM theory needs to be corrected to account for such operating condition. Most of the available skewed wake corrections are based on an equation developed by Glauert [34]. This equation corrects the axial induction factor as follows:

$$a_{skew} = a\left[1 + K_{skew}\frac{r}{R}\cos(\Psi)\right] \qquad (2.26)$$

where K_{skew} is a function of the skew angle and ψ is the azimuth angle. In this case, since the axial induction factor depends on the value of ψ, the BEM equations outlined above need to be solved for each azimuth position. This correction has a limitation primarily due to the fact that it assumes a cylindrical wake, which is true only for lightly loaded rotors. Better predictions of the aerodynamics of wind turbines operating in yaw conditions can be achieved by using alternative methods based on the generalized dynamic wake model [30].

2.5.5 Unsteady aerodynamic effects.

The turbulence associated with the wind and unsteady aerodynamic effects cause rapid fluctuations in the aerodynamic forces acting over the rotor blades, generating vibrations and important material fatigue. In particular, unsteady aerodynamic effects, such as those related to the tower shadow, dynamic stall and dynamic inflow (shortly described below), play a fundamental role on wind turbine operation, and their modelling can improve the accuracy of wind turbine rotor aerodynamic analysis.

2.5.6 Tower shadow.

The wind speed experiences a deficit behind the tower. In downwind turbines, this causes a rapid drop in the power extracted by the rotor blades, and structural vibrations. A model accounting for the tower influence has been developed by Bak et al. [35]. This method models the influence of the tower on the local velocity field at all points around the tower. Fig. 2.12 shows the tower shadow model at a given point. According to this model, the tower wake decays in strength and grows in width as the distance from the tower increases.

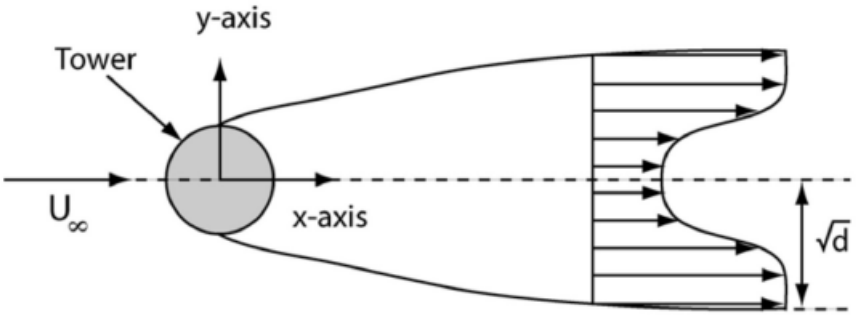

Fig. 2.12 Tower shadow model at a given point. In this picture, U∞ is the freestream wind velocity, and d represents a characteristic length of the model. Image reproduced from [31].

2.5.7 Dynamic stall

When rapid changes in the AoA occur, for example when the rotor blades of a downwind turbine encounter the tower wake or due to the effects of rotor yaw, wind shear and turbulence, turbine blades can experience lift forces that are different (normally larger [36]) than those expected in static conditions. This effect is tied to the blade stall behaviour, and it is normally referred to as dynamic stall. Dynamic stall is an unsteady mechanism than can occur when the AoA of an airfoil increases rapidly from below to above the static stall AoA. In this case, the flow over the airfoil can remain attached at angles of attack above the angle at which steady-state flow separation normally occurs. As shown in Fig. 2.13, under these circumstances, the airfoil can generate a higher lift coefficient than that it would generate in the static cases. In extreme cases, dynamic stall can increase the lift.

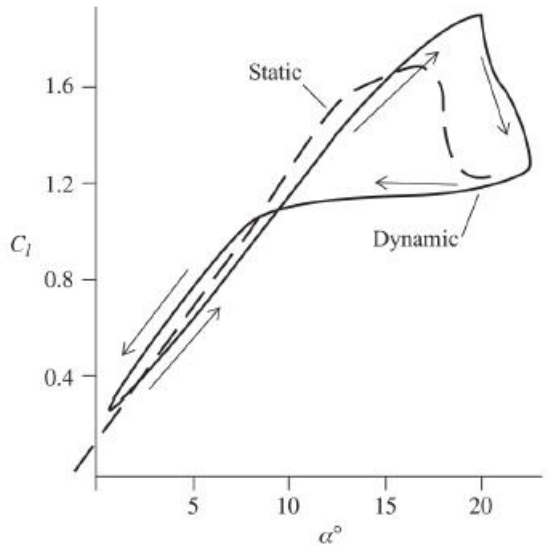

Fig. 2.13 Dynamic stall behaviour. C_l and α represent the lift coefficient and the AoA, respectively. Image reproduced from [37].

coefficient by a factor of three [36]. The flow over the airfoil can then separate suddenly with the result that the lift coefficient drops and the drag coefficient increases. The loads experienced by a blade subject to dynamic stall can be large, causing significant fatigue damage. Dynamic stall also causes sudden variations of the pitching moment, resulting in important loads on the rolling bearings for the blade pitch motion. Several methods have been developed to model dynamic stall, such as those of Gormont [38] and Beddoes [39]. Details on the formulation of the Beddoes's model and its interaction within a BEM code can be found in the AeroDyn's theory manual [31]. Dynamic stall methods are not included in the design framework reported below.

2.5.8 Dynamic inflow.

Dynamic inflow is related to the flow field response to turbulence and changes in rotor operation conditions (for example due to changes in the blade pitch angle or rotor speed). According to steady state aerodynamics, these changes should result in instantaneous changes

in the flow field upstream and downstream of the rotor. However, during rapid changes the flow field cannot respond quickly enough to instantly establish steady state conditions. This results in aerodynamic conditions which may be different from the expected ones. The time scale of dynamic flow effects is on the order of D/U, the ratio of the rotor diameter to the mean ambient flow velocity [29]. Therefore, the time scale of these effects is of the order of about 10 seconds [40]. Phenomena occurring slower than this can be treated using a steady state analysis. More details on dynamic inflow and its modelling can be found in [40–42]. Dynamic inflow methods are not included in the design framework reported below.

2.6 Structural analysis of the rotor blades

The design of wind turbine blades is an involved process mainly due to the complexity of their aerodynamic shape and internal structural characteristics. Indeed, wind turbine blades are made of composite laminates, constituted by anisotropic layup distributed non-uniformly along the blade span. This means that the internal structural layup of composite laminates varies across the blade span from root to tip. As mentioned above, the structural analysis of rotor blades are primarily required to compute mode shape and distributed stiffness and inertial properties needed by wind turbine aeroelastic codes. Moreover, the structural analysis of the blades are needed to verify their structural integrity against ultimate and fatigue limits.

Ultimate load analysis refers to the assessment of material strength (through a stress-strain analysis), blade tip deflection and structural stability (i.e., buckling), while fatigue load analysis concerns fatigue strength. The extraction of the structural properties of the blade and the stress-strain, blade tip deflection and buckling analyses are normally carried out using structural codes. Fatigue calculations involve the use of specific algorithms to process load histories in order to determine the damage accumulation. The initial part of this section deals with different methods commonly used to perform the structural analysis of wind turbine blades and fatigue calculations.

The realistic ultimate and fatigue loads, that turbine components are subjected to, need to be accurately assessed. Such loads are normally generated by running a series of aeroelastic simulations under different operating and environmental conditions, covering most of the situations that wind turbines likely experience during their lifetime. As mentioned in Chapter 1, these conditions are prescribed by standards, such as the IEC standard [43]. Wind conditions considered by these standards are normally fed into aeroelastic codes by means of wind input files. The concluding part of this section will describe the structure of such files, and explain how they can be generated.

2.6.1 Methods for the structural analysis of wind turbine blades

Finite element method (FEM) codes, such as ANSYS [44], Abaqus [45], SolidWorks [46] and NuMAD [47], can be used to perform the structural analysis of wind turbine blades, accurately accounting for complex geometric shapes and composite structural layup. FEMs rely on numerical approximation techniques that divide a component or structure into discrete regions (the finite elements) and the response is described by a set of functions that represent the displacements or stresses in those regions [48]. These models are able to accurately provide the span-variant properties of the blades, and describe the strain-stress fields in detail. The use of FEM techniques is however computationally expensive, requiring the generation of a computational mesh, and complex post-processing. In the preliminary design stages, where a huge number of different configurations may be evaluated, FEM approaches may become impractical. Therefore, the structural analysis in the aeroelastic design optimization of wind turbine rotors generally relies on simpler and faster models. The rest of this section will review some of these simplified structural models tailored towards composite rotor blades, and featuring various solution techniques.

PreComp [49] is a popular NREL code developed to provide span-variant structural properties for composite blades. These structural properties encompass: flap, lag (edgewise), axial (with

respect to the blade pitch axis), and torsion stiffness's, as well as orientation of principal axes, density, and moments of inertia. This code is based on the classical lamination theory (CLT) with a shear-flow approach. Details on the CLT and the shear-flow theory can be found respectively in [50, 51] and [52]. It should be noted that PreComp cannot be used to perform stress-strain analysis. Therefore, in the framework of this research, alternative structural codes, not based on FEMs, yet featuring stress-strain analysis capabilities, have been reviewed.

Co-Blade [53] is a computationally efficient open source structural analysis and design code developed by Sale. This code includes all of the same capabilities of PreComp, adding analysis of load induced strain, stress, deflection, buckling, optimization capabilities, and graphical post-processing capabilities. Making use of a blend of CLT, Euler-Bernoulli theory [52, 54, 55] and shear flow theory applied to composite beams, Co-Blade predicts both the distributed structural properties of composite wind turbine blades, and their deformation and material stress fields. The Co-Blade's technical approach models the turbine blade as a cantilever beam subject to aerodynamic loads, self-weight, buoyancy, and centrifugal forces. As a consequence, the beam undergoes bending, axial deflection (i.e., tension and compression along the longitudinal axis of the beam), and twist (i.e. torsion about the longitudinal axis of the beam). The linear differential equations of equilibrium for a cantilever beam are then used to determine the shear force and bending moment distributions along the beam length. Co-Blade considers the beam cross sections are assumed to be thin-walled, closed, and single- or multi-cellular. The cross-section of the cantilever beam is discretized as a connection of flat composite laminates, as illustrated in Fig. 2.14.

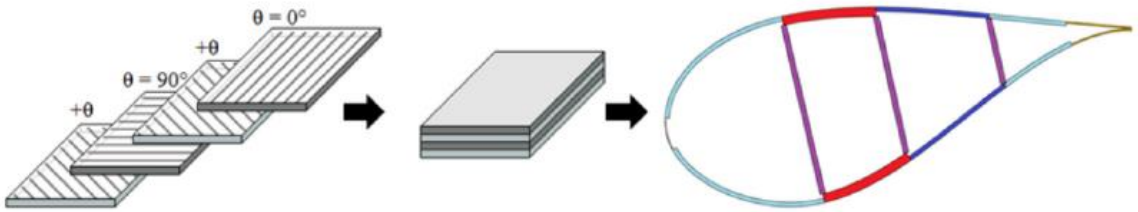

Fig. 2.14 Modelling of the turbine blade cross-section. Each section is discretized as a connection of composite laminate plates, each made up of a number of different laminas (θ represent the orientation of each lamina's principal material direction with respect to the blade axis). Image reproduced from [53].

Although each composite laminate is a stack of a number of different laminas (each characterized by its own material and constitutive properties), the CLT is used to evaluate the effective mechanical properties (i.e., Young's modulus, shear modulus, Poisson's ratio, thickness, and density) of each laminate, treating it as a single structural element. Therefore, the beam cross-section is made up of a number of discrete areas, or panels, of homogeneous material (represented through different colours in Fig. 2.14). The panels, made up of consistent flat composite laminates, are characterized by the effective mechanical properties computed via CLT. Each panel then contributes to the global cross-sectional properties, which are computed by the method of Young's modulus weighted properties [54, 55]. Once that global cross-sectional properties are known, the deflections and the beam effective axial stress and effective beam shear stress are computed under the assumption of a Euler-Bernoulli beam. The calculation of the beam effective shear stress is based on a shear flow approach. The distributions of the effective beam stresses from the Euler-Bernoulli theory are eventually converted into the equivalent in-plane distributed loads on the flat composite laminates, so that the strains and stresses of each lamina can be recovered by means of CLT. Co-Blade follows

the approach described in [56, 57] to perform the linear buckling analysis of the blade. In this approach the top and the bottom surfaces of the blade are modelled as curved plates subject to a combination of compression and shear loads, while the shear webs (connecting the top surface to the bottom one) are modelled as flat plates subject to combined bending and shear. Practically, panel buckling is treated by means of a buckling criteria R expressed by a dimensionless number which is lower than 1 if the effective stresses in a panel have not exceeded the critical buckling stresses.

Another simple and fast structural code has been developed and presented by Ashuri et al. [58]. This code, based on the Euler-Bernoulli theory, enables both the extraction of structural properties of a composite wind turbine blade and the calculation of its bending stress field. In fact, unlike Precomp, this code includes the calculation of the cross-sectional area moments of inertia, allowing one to determine the bending stresses σ. For this purpose, the classic formula for determining σ, in a beam under simple bending, can be used as follows:

$$\sigma = \frac{M_y}{I_x} \qquad (2.27)$$

where M is the moment about the neutral axis, y is the perpendicular distance to the neutral axis, and Ix is the cross-sectional area moments of inertia about the neutral axis.

As mentioned above, blade mode shapes are required to perform rotor aeroelastic simulations by means of aeroelastic codes. Moreover, to avoid blade resonance issues, rotor blades should be designed considering their natural frequencies. As explained in Chapter 6, the first natural frequency of the blade should be above the maximum rotor blade passing frequency. All the structural codes described in this section cannot cope with the calculation of either the blade mode shapes or the blade natural frequencies. The pre-processor BModes [59] is a NREL tool able to generate coupled modes and natural frequencies for a turbine blade or a tower. BModes uses distributed inertial and stiffness properties of the blade and tower along their longitudinal

axis. For blade mode shapes calculation, BModes also requires the rotational speed of the blade to calculate the rotational stiffening and its pitch angle as input. From the solution of the associated eigenvectors, polynomial expressions of the mode shapes are calculated. The calculation of the natural frequencies is carried out in the same way, including the stiffening effects of rotation.

2.6.2 Fatigue

Fatigue is defined as the progressive and localized structural damage that occurs when a material is subject to cyclic loading. Due to the spatiotemporal variability of the wind and the rotation of the rotor, wind turbine components, such as the rotor blades, tower and drive train, indeed experience cycling loads throughout their lifespan, and therefore they need to be designed against fatigue. The most common approach to design wind turbine mechanical parts against fatigue is to keep structural stress below threshold of fatigue limit, normally represented by a parameter indicating the fatigue damage accumulation.

Fatigue analysis for wind turbines is typically carried out by running a large number of aeroelastic (time-domain) simulations under different wind conditions, determining the fatigue loads expected over the lifetime of the turbine. Fatigue loads on each primary component of the turbine is then post-processed. MLife [60] is a NREL code, created to compute fatigue estimates resulting from time-series load data files. This code accumulates fatigue damage due to fluctuating loads. These fluctuating loads are broken down into individual hysteresis cycles each characterized by a load mean and range, using the rain flow counting method according to the ASTM standard [61]. In practice, the rain flow counting algorithm reduces a complex spectrum of varying loads into a simple set (or series) of cycles defined by a given mean and amplitude. MLife assumes that the fatigue damage accumulates linearly and independently for each of these cycles according to the Miner's rule [62]. Thus, the total damage resulting from all cycles is given by:

$$D = \sum_i \frac{n_i}{N_i(L_i^{RF})} \qquad (2.28)$$

where L_i^{RF} denotes a given cycle's load range about a fixed load-mean value and $N_i(L_i^{RF})$ represents the number of cycles, characterized by L_i^{RF}, that would lead to failure. n_i represents the actual count of cycles characterized by L_i^{RF}. When n_i is equal to $Ni(L_i^{RF})$ failure occurs, and this corresponds to D equal to 1. Load ranges are related to cycles to failure by means of the S-N curve (or Woler curve) which can be modeled as follows:

$$N_i = \left(\frac{L^{ult} - |L^{MF}|}{\left(\frac{1}{2} L_i^{RF}\right)} \right)^m \qquad (2.29)$$

where L^{ult} is the ultimate design load of the component, L^{MF} is the fixed lead mean and m is the Woler exponent, depending on the considered component.

CHAPTER 3

RESEARCH METHODOLOGY

3.1 Fundamental Equations

Laws of conservation of physics are represented by governing equations of fluid flow through mathematical statements.

- According to newton's 2nd law, Summation of forces on a fluid particle is equal to the change in rate of momentum.
- Fluid mass is conserved.
- According to 1st law of thermodynamics, rate of change of energy is equal to the summation of heat added to a fluid particle and total work done on it.

Using Navier Strokes equations, these conservation laws can be applied to a control volume or a small fluid element.

3.1.1 Navier Stokes Equations

As shown by Pope et al. [42], theoretical basis of the problems starts from conservation of mass and momentum as follows :

$$\frac{\partial \rho}{\partial t} + \nabla . (\rho \vec{v}) = 0 \qquad (3.1)$$

$$\rho \frac{\mathrm{D}U_j}{\mathrm{D}t} = \frac{\partial \tau_{ij}}{\partial x_i} - \rho \frac{\partial \Psi}{\partial x_j} \qquad (3.2)$$

where,

$\vec{v}$ = 3-D velocity vector

$\partial\tau_{ij}$ = stress tensor

Ψ = external body force vector

Presence of non-linearities restricts the direct numerical solution to these equations which leads to assumptions of turbulent viscosity theory in this solution. Averaged form of continuity and momentum equations can be written using substitutions of the Reynolds decomposition as

$$U\,(x,\,t) = \{U\,(x,\,t)\} + u\,(x,\,t) \tag{3.3}$$

where, the vector x represents stream wise in x direction, span wise in y direction, and vertical in z direction.

The stress tensor is shown below,

$$\tau_{ij} = P\delta_{ij} + \mu\left(\frac{\delta U_i}{\delta x_j} + \frac{\partial U_i}{\partial x_j}\right) \tag{3.4}$$

3.1.2 k-ω Standard model

Wilcox [56] developed the k- ω Standard model to analyse turbulent viscosity (Menter et.al.) using transport equations of k- ω, the turbulence kinetic energy and ω, the turbulence frequency. These transport equations are:

$$\frac{D(\rho k)}{Dt} = \mathrm{P} - \beta^{*}\rho\omega\mathrm{k} + \frac{\partial}{\partial x_j}\left[\left(\mu + \sigma_k\frac{\rho k}{\omega}\right)\frac{\partial k}{\partial x_j}\right] \tag{3.5}$$

$$\frac{D(\rho\omega)}{Dt} = \frac{a\omega}{k}\mathrm{P} - \beta\rho\omega^{2} + \frac{\partial}{\partial x_j}\left[\left(\mu + \sigma_\omega\frac{\rho k}{\omega}\right)\frac{\partial \omega}{\partial x_j}\right] \tag{3.6}$$

k-ω turbulence model equations used RANS equation as shown above to solve three dimensional turbulent steady state incompressible flow.

3.2 Model Description

SolidWorks was used to develop the geometry of GE 1.5xle reference turbine [55]. Further it was exported to Ansys Design Modeler, where its domain geometry was developed. GE 1.5xle

turbine is one of the best in its class and hence is widely used. Steady state one way FSI (Fluid-Structure Interaction) analysis is used to show deformation due to aerodynamic loading of wind turbine. Blade length is 43.2 metres long which starts with a cylindrical shape at the root and further transitions to S818, S825, S826 airfoils at root, body and tip respectively. The pitch of this blade varies as a function of radius which gives it a twist and has pitch angle of 4 degrees at blade tip. All the technical details of the GE 1.5xle blade is given in table 3.1.

Table 3.1 Technical details of GE's 1.5xle [55]

Electrical parameters	
Voltage	690 V
Frequency	50/60 Hz
Tower	
Hub Height	80 m
Rated Capacity	**1500 W**
Rated Wind Speed	11.5 m/s
Cut in Wind Speed	3.5 m/s
Cut out Wind Speed	20 m/s
Rotor	
Rotor Diameter	86.4 m
Swept Area	5348 m^2

3.2.1 Governing equations

Time-averaged momentum equations (RANS equations [20]) in accordance with time-averaged continuity are the governing equations of fluid flow. These relations are as follows:

$$\frac{\partial \bar{u}_i}{\partial x_i} = 0 \qquad (3.7)$$

$$\frac{\partial \bar{u}_i}{\partial t} + \bar{u}_j \frac{\partial \bar{u}_i}{\partial x_j} = \frac{1}{\rho} \frac{\partial}{\partial x_j} \left(\tau_{ij}{}^{eff}\right) + \bar{G}_i \qquad (3.8)$$

$$\tau_{ij}{}^{eff} = - \acute{p}\delta_{ij} + \mu\left(\frac{\partial \bar{u}_i}{\partial x_j} + \frac{\partial \bar{u}_j}{\partial x_i}\right) - \rho\, u'_i u'_j \qquad (3.9)$$

Last term in equation 3 is Reynold's stress which is modelled by turbulence model. The standard k-ω model used here is a turbulence model in which turbulence viscosity is related to turbulence kinetic energy and turbulence frequency as shown below:

$$\mu_t = \frac{\rho k}{\omega}$$

3.2.2 Boundary conditions

Inlet and outlet boundary conditions are set as velocity inlet and pressure outlet respectively. Boundaries are set to be as 90 m in front and 180 m behind the rotor respectively. Dimensional angles are set as 60 degrees each. Dimensional radius is set to be at 120 m and 240 m for velocity inlet and pressure outlet respectively.

The fluid is taken as incompressible air of density 1.225 kg/m^3 at 25°C and its reference pressure is considered as 101325 pa.

3.3 CFD Designing

It's a tool of modelling a fluid flow around a blade by disintegrating the geometry into various small cells which comprises a mesh. An algorithm is developed for each cell to compute for

the fluid flow around the cells. Navier-strokes equations or Euler can be used for the computation depending on the nature of flow.

It comprises of various steps:

Step 1: Problem Identification

- Define goals and objectives
- Identify the domain in which it exists.

Step 2: Pre- processing

- Geometry construction
- Mesh formation
- Physics setup
- Solver setting

Step 3: Solve Equation

- Calculate solution

Step 4: Post-processing

- analyse results

3.3.1 Model Formation

A modelling software called solid works is used to generate GE's 1.5xle turbine blade using the coordinates from [17]. Model generated was further imported to Ansys software. Blade geometry imported to Ansys is shown in figure 3.1.

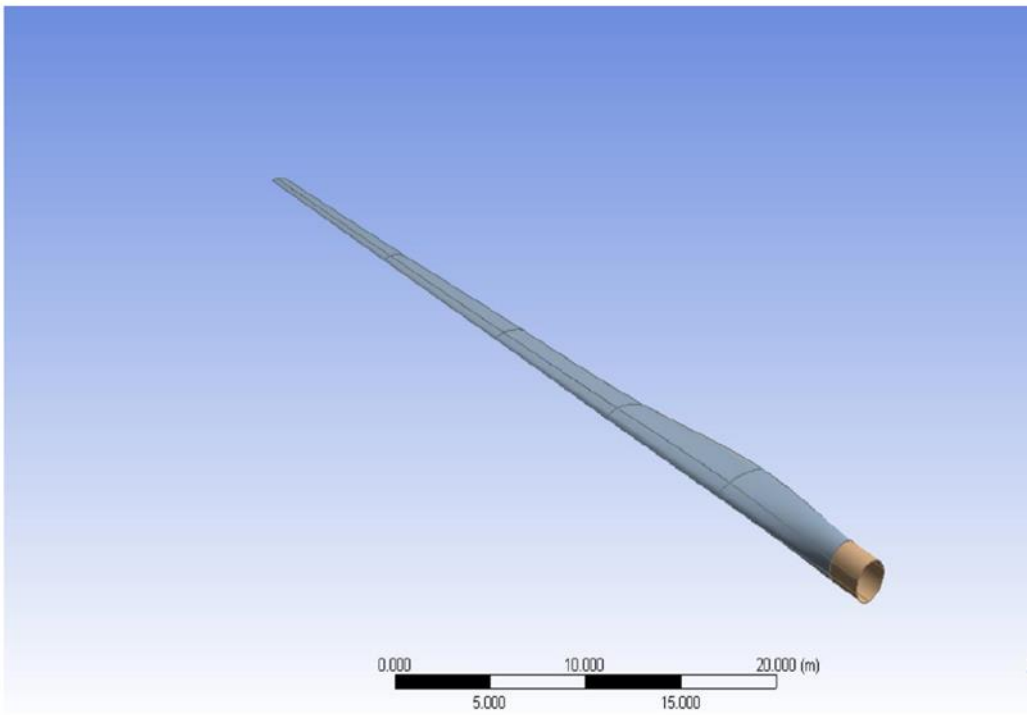

Figure 3.1 Blade Geometry of GE's 1.5xle

3.3.2 Meshing

Geometry is break down into smaller parts such as nodes, elements etc using discretization scheme. This resultant discretized geometry which comprise of many smaller computations parts is termed as mesh.

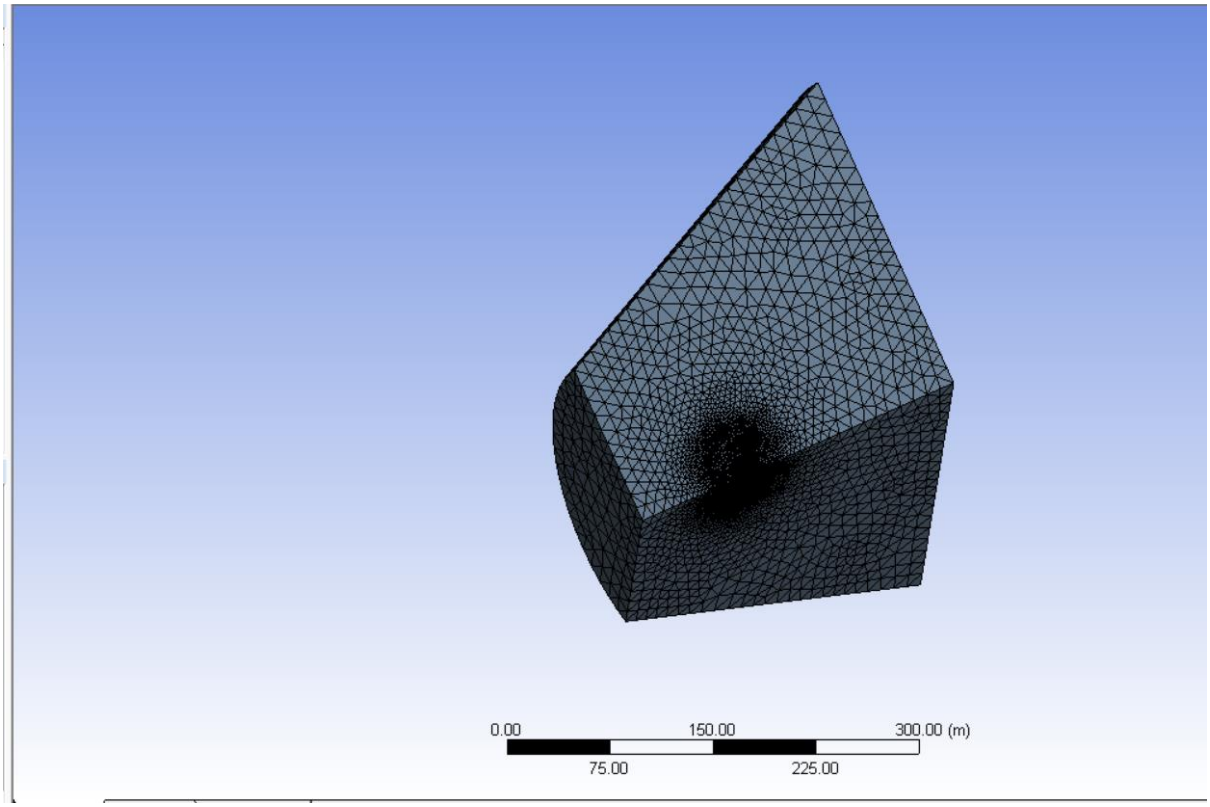

Figure 3.2 Tetrahedral Mesh

3.3.3 Mesh Metrics

Mesh metrics is use to judge the quality of mesh as a bad mesh can lead to bad results. Maximum skewness should be kept lower than 0.95 for a good quality mesh. Having poor cells or elements can lead to false simulation results. The following table 3.2 can help you gauge the quality of your mesh.

Table 3.2 Skewness range

Skewness:

Excellent	Very Good	Good	Sufficient	Bad	Inappropriate
0-0.25	0.25-0.50	0.50-0.80	0.80-0.95	0.95-0.98	0.98-1.00

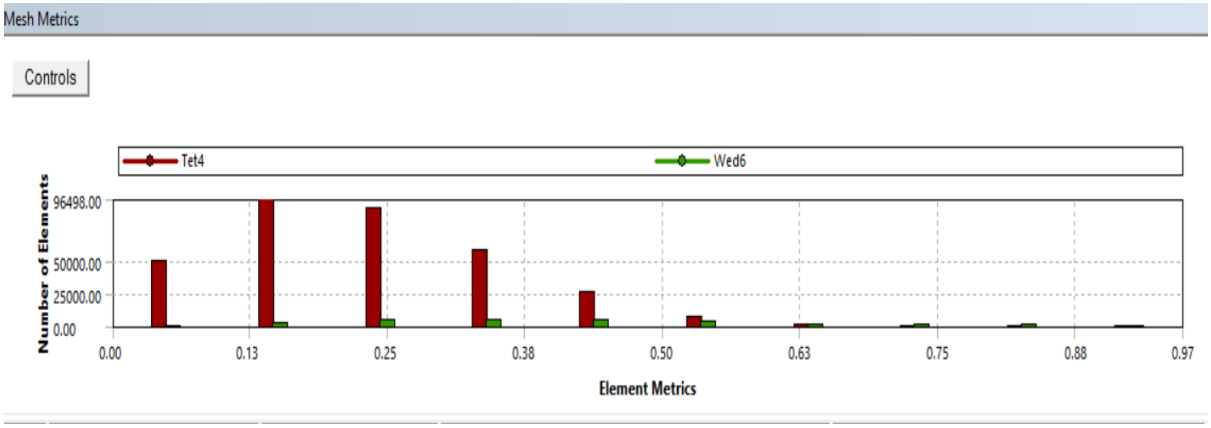

Figure 3.3 Skewness

As shown in above figure 3.3, skewness for our mesh is below 0.5 for most of the elements which is good and assure it as a good quality mesh.

3.4 FEA Simulation

Now the solid mechanics aspects of wind turbine come into play for which FEA simulation is performed. Pressure load which are calculated in the fluent are imported to Ansys Mechanical and stress and deformations on the blade are calculated.

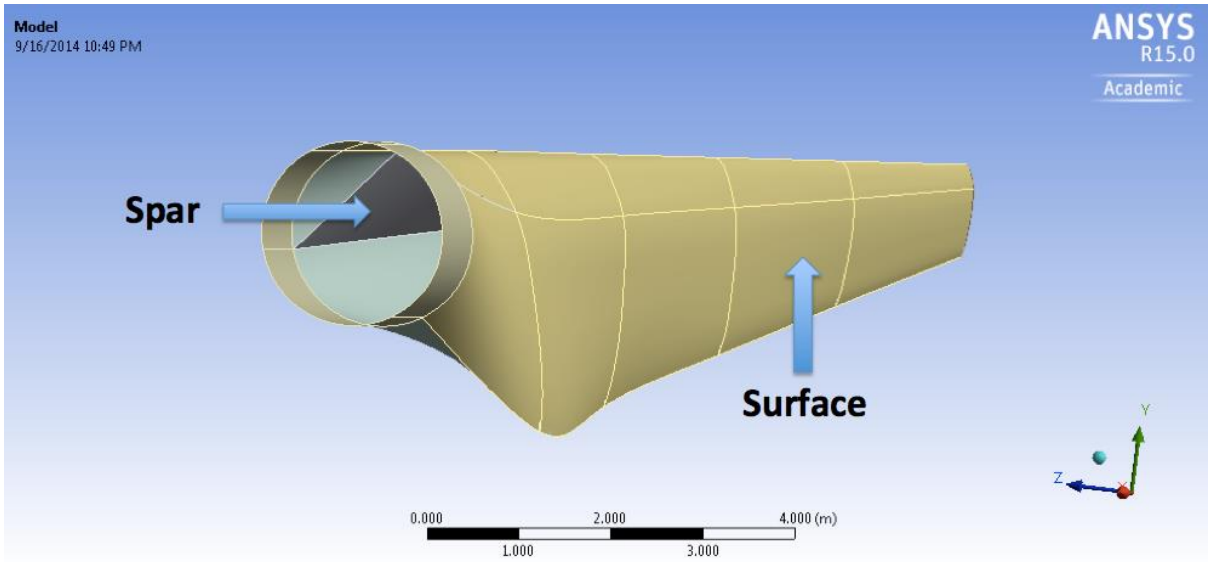

Figure 3.4 Wind turbine blade structure

Blade is composed of an outer surface and an inner spar as shown in above figure 3.4.

Composite materials are used now a day to produce wind turbine blades so as to reduce the weight of huge machines. For the simplification of structural analysis, we assume the following material properties of our composite material.

Table 3.3 These values are approximated as the composite properties which are generally found in real wind turbine blades.

Density (kg/m^3)	1550
Young's Modulus-X (Pa)	1.1375E+11
Young's Modulus-Y (Pa)	7.583E+09
Young's Modulus-Z (Pa)	7.583E+09
Poisson's Ratio-XY	0.32
Poisson's Ratio-YZ	0.37
Poisson's Ratio-XZ	0.35
Shear Modulus-XY (Pa)	5.446E+09
Shear Modulus-YZ (Pa)	2.964E+09
Shear Modulus-XZ (Pa)	2.964E+09

Proper meshing of wind turbine blade is performed in Mechanical as shown below.

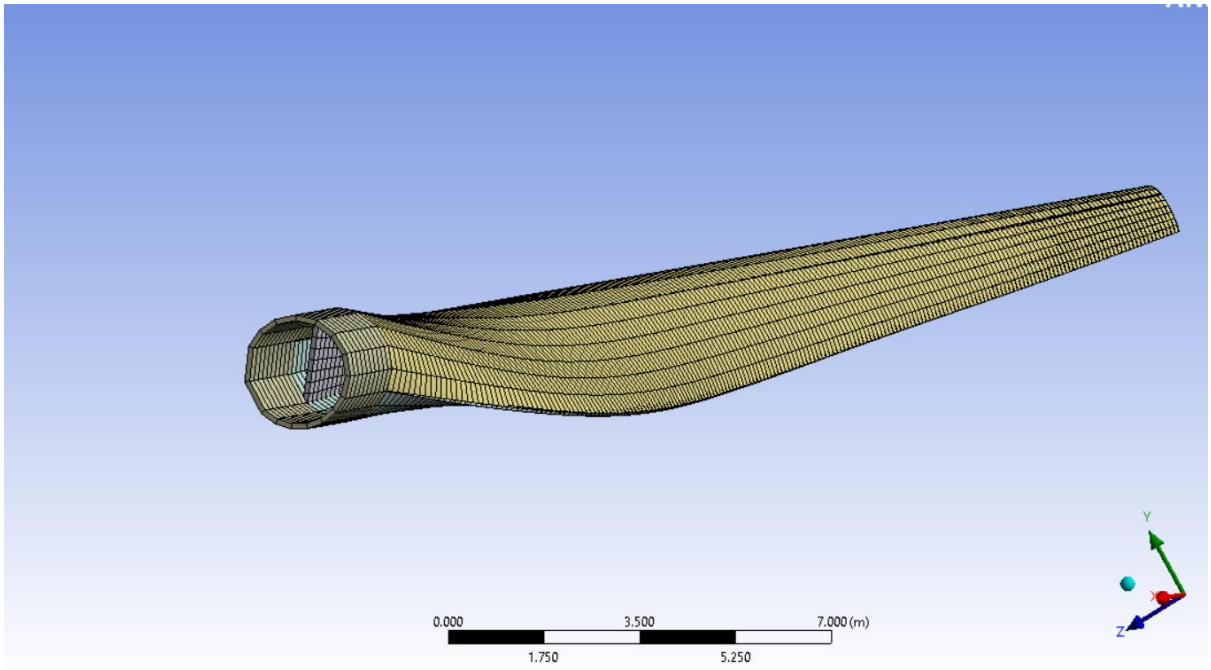

Figure 3.5 Mesh of wind turbine blade structural analysis

3.5 Numerical Setup

Summary of steps undergone in CFD

1. Solution Methods
    a. Select Coupled option for Scheme
    b. Standard pressure is selected
    c. Check Pseudo transient and High Order term relaxation
2. Set Monitors
    a. Residuals in all parameters is changed to 1e-6.
    b. Surface monitor is created
    c. Check Plot & write
    d. Select Blade surface

3. Solution Initialization
    a. Choose Standard initialization
        i. Compute from inlet
4. Run Calculation
    a. Iterations = 1500.
    b. Initialize solution
    c. Run calculation

In FEA for structure analysis, to obtain the numerical solution, click solve. ANSYS formed the stiffness matrix for each element, assembled the global stiffness matrix and inverted it to get the nodal displacements. This is the bulk of the computation that ANSYS performs. All the results that we look at next such as the deformed shape and the stresses are derived from these nodal displacements.

CHAPTER 4

RESULTS AND DISCUSSION

4.1 Examine the effects of scaling on structural parameters

The GE's 1.5xle wind turbine is used as large turbine and its scaled down model to 4 times is simulated in Ansys software for CFD and FEA analysis. After simulation is completed for both at various speed, structural parameters resulted from simulation and results predicted by similarity theory as stated before is compared for further analysis. Several simulations were performed at different wind speeds which is set to be 7,10,12,15,17.5 and 20 m/s. Fig. 4.1 shows the force reaction resulted after simulation for large scale turbine(LST) and the predictions by similarity theory which were calculated from scaling relations as shown in Table 2.1. Table 4.1 shows the Force reaction values for large scale turbine, values predicted by similarity theory and small scale turbine. Here, Values obtained by simulating the large scale turbine are in complete agreement with the results predicted by similarity theory as the relative error between them is below 1%.

Table 4.1 Values of Force Reaction from LST and Predicted by Similarity

S. No.	Wind Speed (m/s)	Force Reaction $_{LST}$, (kN)	Force Reaction Similarity Theory (kN)	Force Reaction $_{SST}$ (kN)	Error (%)
1	7	1578	1578.9	98.68	0.057
2	10	1579	1579.56	98.72	0.036

3	12	1579.8	1580.36	98.77	0.035
4	15	1581.2	1581.25	98.82	0.0032
5	17.5	1582.2	1582.59	98.91	0.025
6	20	1583.2	1583.75	98.99	0.034

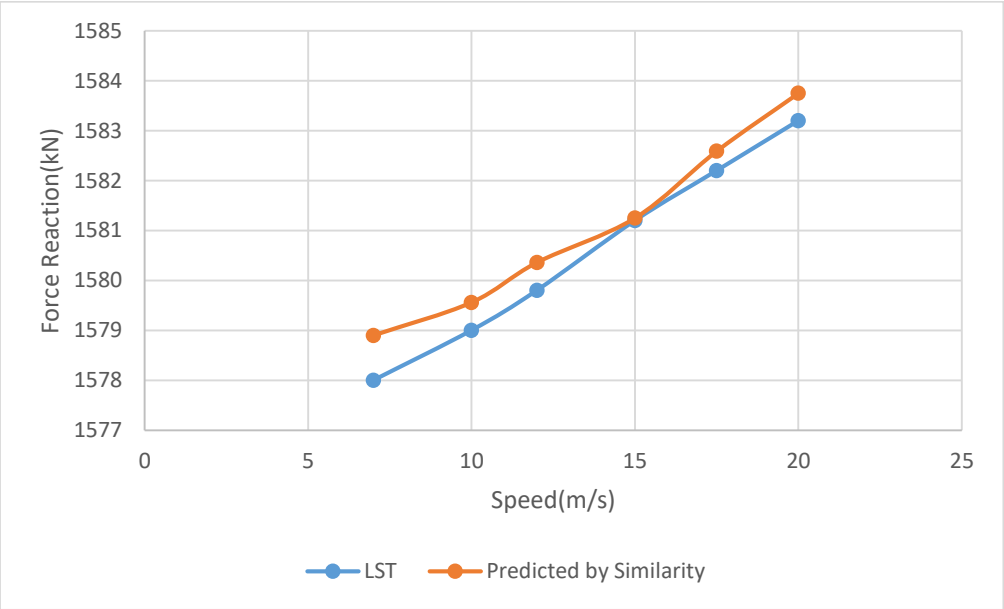

Figure 4.1 Comparison of Force Reaction value obtained from simulation and values predicted by similarity theory

Table 4.2 shows the blade mass values for large scale turbine, values predicted by similarity theory and small scale turbine. Error between blade mass values of large scale turbine and values predicted by similarity theories are found to be less than 1% which further confirm that results of the simulation completely follow the values predicted by similarity theory. In fig 4.2, a graph is plotted between the values of LST and values predicted by similarity theory to show the variation at different wind speeds.

Table 4.2 Comparison of Blade Mass from LST and Predicted by Similarity Theory

S. No.	Wind Speed (m/s)	Mass $_{LST}$, (kg)	Mass $_{Similarity\ Theory}$ (kg)	Mass $_{SST}$ (kg)	Error (%)
1	7	22473	22668.51	354.19	0.87
2	10	22473	22668.51	354.19	0.87
3	12	22473	22668.51	354.19	0.87
4	15	22473	22668.51	354.19	0.87
5	17.5	22473	22668.51	354.19	0.87
6	20	22473	22668.51	354.19	0.87

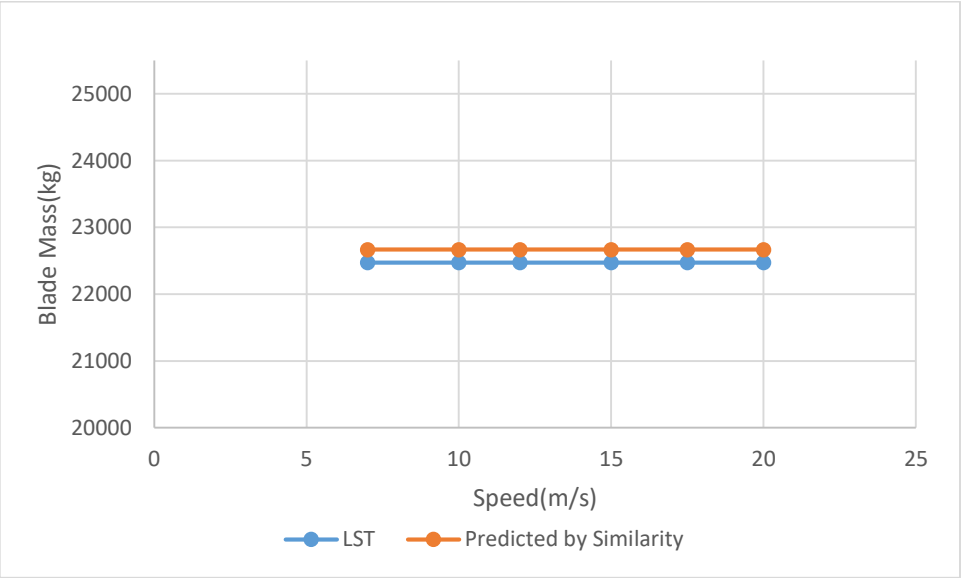

Figure 4.2 Comparison of Blade Mass value obtained from simulation and values predicted by similarity theory

Table 4.3 shows the Equivalent Stress values for large scale turbine, values predicted by similarity theory and small scale turbine. Error between equivalent stress values of large scale turbine and values predicted by similarity theories are found to be less than 1% for all wind speed except for 7 m/s for which it is found to be close to 8%. This large variation between the values of large scale turbine and values predicted by similarity theory is due to incompatibility between the fluid flow in real condition and fully turbulent model for small scale turbine. In fig 4.3, a graph is plotted between the values of LST and values predicted by similarity theory to show the variation at different wind speeds.

Table 4.3 Comparison of Equivalent Stress from LST and Predicted by Similarity

S. No.	Wind Speed (m/s)	Equivalent Stress $_{LST}$, (MPa)	Equivalent Stress Similarity Theory (Mpa)	Equivalent Stress $_{SST}$, (MPa)	Error (%)
1	7	19.561	21.12	1.32	7.9
2	10	28.722	29	1.81	0.96
3	12	34.13	34.813	2.17	2.0
4	15	40.991	41.195	2.57	0.497
5	17.5	44.359	45.024	2.81	1.49
6	20	45.914	46.832	2.92	1.9

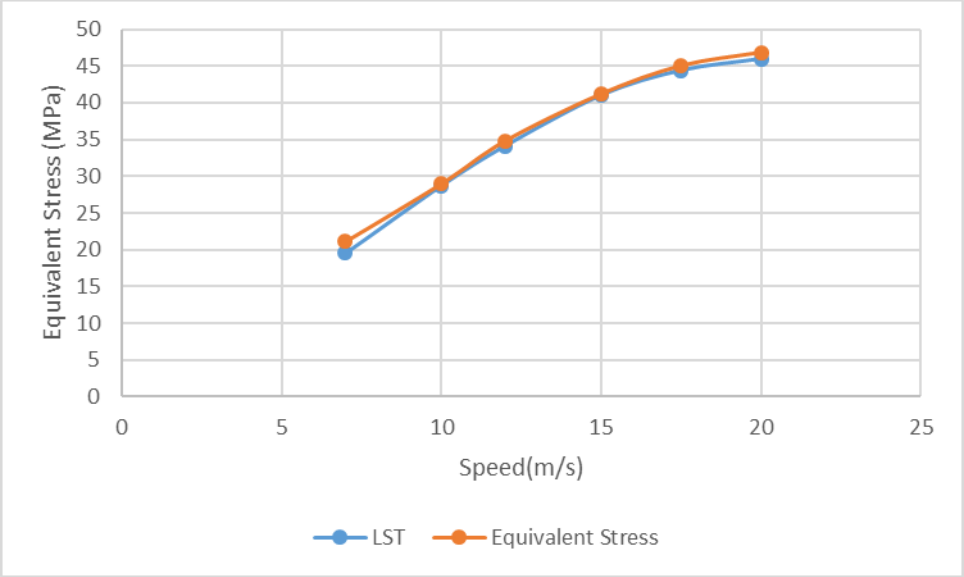

Figure 4.3 Comparison of Equivalent Stress value obtained from simulation and values predicted by similarity theory

Table 4.4 shows the Moment values for large scale turbine, values predicted by similarity theory and small scale turbine. Error between moment values of large scale turbine and values predicted by similarity theories are found to be less than 3% for all wind speed except for 7 m/s for which it is found to be close to 7%. This large variation between the values of large scale turbine and values predicted by similarity theory is same as that explained in equivalent stress condition which is due to incompatibility between the fluid flow in real condition and fully turbulent model for small scale turbine. In fig 4.4, a graph is plotted between the values of LST and values predicted by similarity theory to show the variation at different wind speeds.

Table 4.4 Comparison of Moment from LST and Predicted by Similarity

S. No.	Wind Speed (m/s)	Moment $_{LST}$, (N-m)*10^{06}	Moment $_{Similarity\ Theory}$ (N-m) *10^{06}	Moment $_{SST}$, (N-m)*10^{06}	Error (%)
1	7	1.2147	1.3	0.02	7.02
2	10	2.042	2.035	0.031	0.343
3	12	2.5235	2.537	0.039	0.534
4	15	3.0998	3.138	0.049	1.29
5	17.5	3.348	3.399	0.053	2.42
6	20	3.529	3.559	0.055	0.85

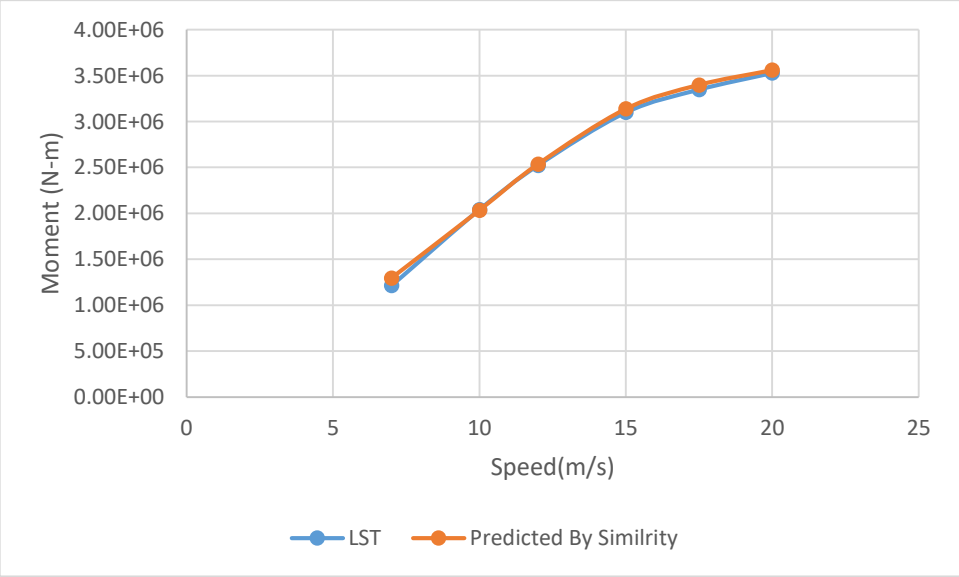

Figure 4.4 Comparison of Moment value obtained from simulation and values predicted by similarity theory

From the results obtained in this section, mass and moment increases with the cube of change in rotor diameter as stated in the traditional similarity theory rules whereas force reaction and stress increases with square of change in rotor diameter as per similarity theory rules. Also keep in mind that, Similarity theory rules are valid only when the flow condition such as triangles of velocity and relative velocity angles are kept same for both large and small wind turbines.

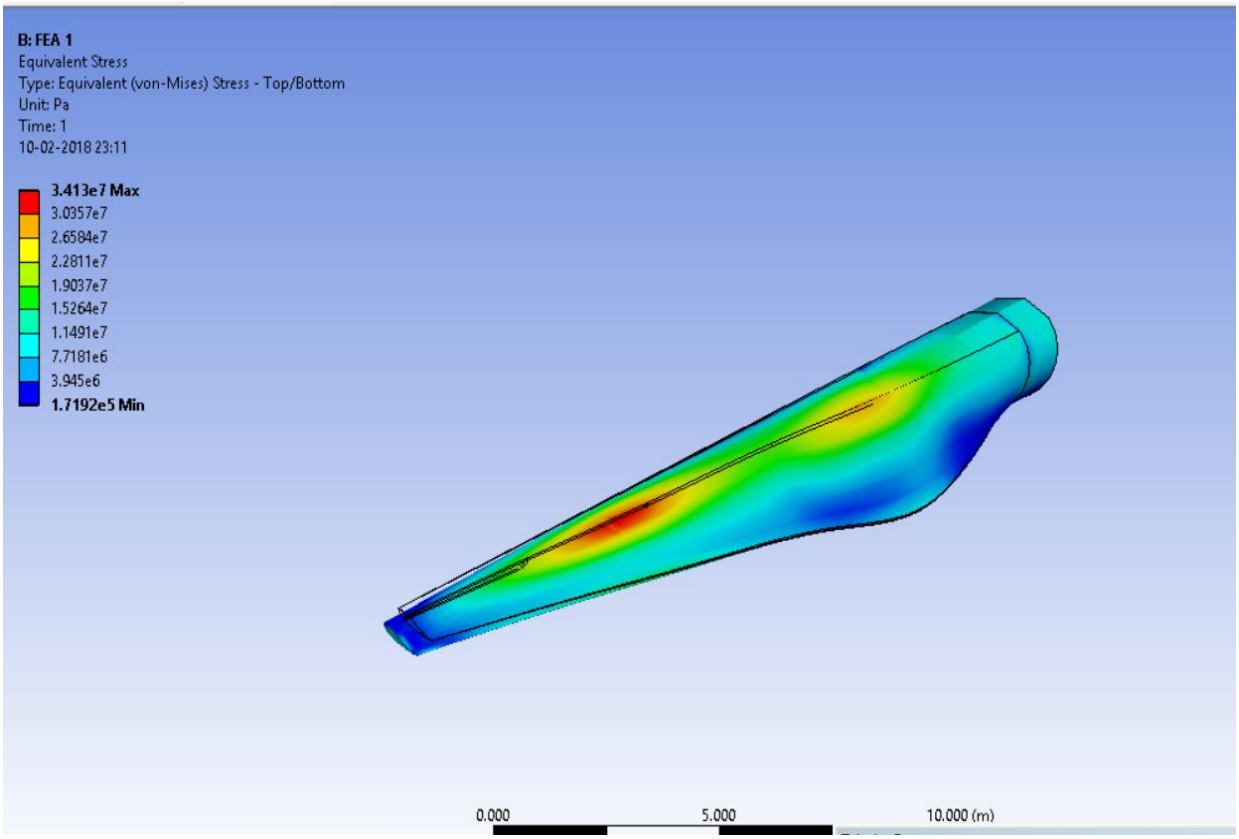

Figure 4.5 Equivalent Stress variation cross-section of blade at velocity 12m/s

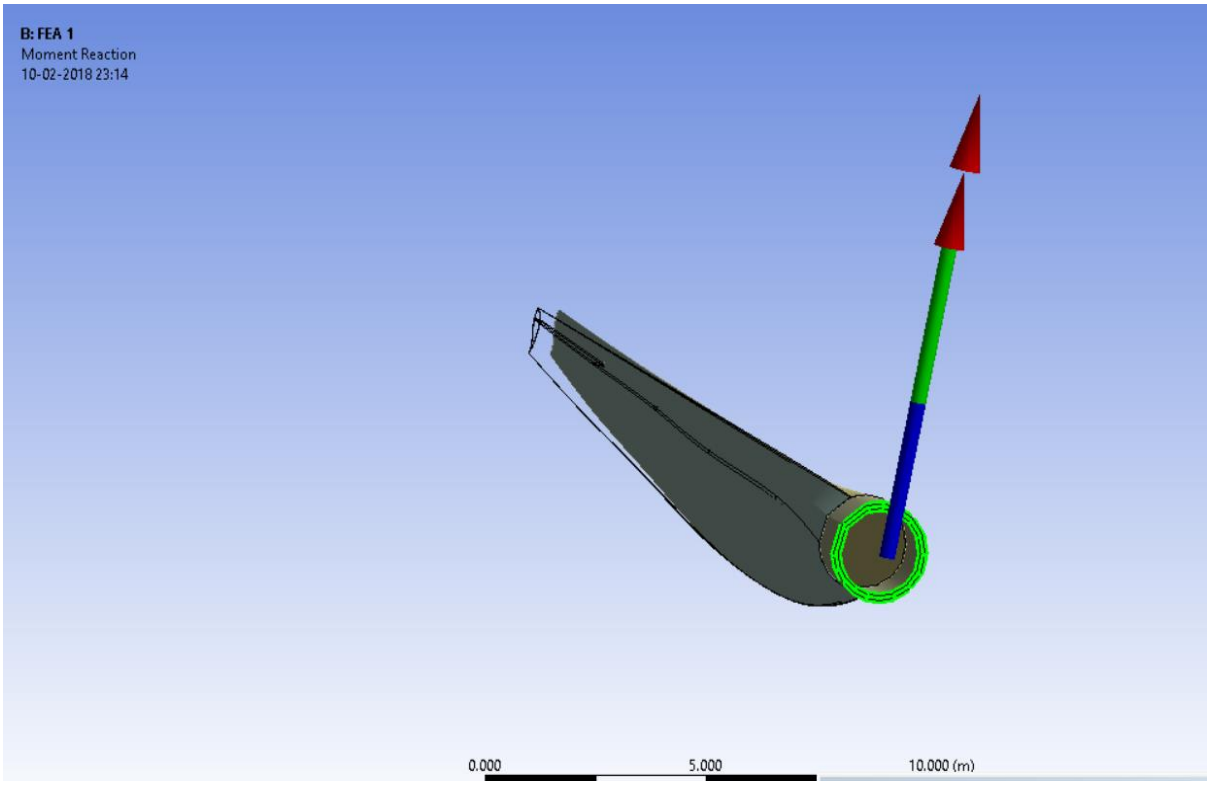

Figure 4.5 Moment and Force Reaction of Blade for velocity 12 m/s

CHAPTER 5

CONCLUSION

5.1 Summary

In this thesis, effects of scaling the wind turbine blade on various structural parameters which include Force reaction, Blade mass, Equivalent stress and moment were investigated on the blade. Values predicted by similarity theory are in complete agreement with the results of the simulation for all wind speeds except for low wind speed where there is a visible difference between predictions of similarity and simulation results. Reason behind this difference is due to the incompatibility between fully turbulent model employed to simulate the flow and the real flow regime which is not fully turbulent in some regions of blade span. Further conclusion can be drawn from this investigation

- Increase in Force reaction due to scaling up of wind turbine increases with square of change in rotor diameter.
- Increase in mass due to scaling up of wind turbine increases with cube of change in rotor diameter which necessitates the development of stronger and lighter materials so as to construct large wind turbine blades to extract more energy without increasing much of the blade weight and increase cost and complexity.
- Increase in moment due to scaling up of wind turbine increases with cube of change in rotor diameter which limits the length of wind turbine blades.
- Increase in equivalent stress due to scaling up of wind turbine increases with square of change in rotor diameter.
- Structural analysis is unaffected by closely spaced rotor.

5.2 Future Works

Further study can be done in multi rotor wind turbine(MRWT) design and scaling effects are investigated to improve its design for better performance of wind turbine blade. From economic prospects, cost optimization study can be done for wind turbine.

REFERENCES

1. Global Wind Energy Council. Global Wind Report 2013 - Annual market update. Technical report, GWEC, Brussels, Belgium, 2013.
2. P. Brondsted. Introduction. In P. Brondsted and R. P. L. Nijssen, editors, Advances in wind turbine blade design and materials, volume 47 of Energy. Woodhead Publishing Limited, 2013. ISBN 978-0-85709-426-1.
3. T. Ashuri. Beyond Classical Upscaling: Integrated Aeroservoelastic Design and Optimization of Large Offshore Wind Turbines. PhD thesis, TU Delft, 2012.
4. G. Sieros, P. Chaviaropoulos, J. D. Sorensen, B. H. Bulder, and P. Jamieson. Upscaling wind turbines: theoretical and practical aspects and their impact on the cost of energy. Wind Energy, 15(1):3–17, 2012.
5. TPI Composites, "Innovative Design Approaches for Large Wind Turbine Blades Final Report," SAND2004-0074, Sandia National Laboratories, 2004.
6. Griffin, D. A., “WindPACT Turbine Design Scaling Studies Technical Area 1 -- Composite Blades for 80- to 120-Meter Rotor,” 21 March 2000 - 15 March 2001, NREL Report No. SR-500-29492, 2001.
7. Griffin D.A. and T.D. Ashwill, “Alternative Composite Materials for Megawatt-scale Wind Turbine Blades: Design Considerations and Recommended Testing,” 2003 ASME Wind Energy Symposium at the 41st AIAA Aerospace Sciences Meeting and Exhibit, AIAA-2003-0696, Reno, NV, January 2003.
8. Hillmer, “Aerodynamic and Structural Design of Multi-MW Wind Turbine Blades beyond 5MW,” Science of Making Torque from the Wind Conference, 2007.
9. Kooijman, H.J.T., C. Lindenburg, D. Winkelaar, and E.L. van der Hooft, “DOWEC 6 MW Pre-Design: Aero-elastic modeling of the DOWEC 6 MW pre-design in

PHATAS," ECN-CX--01-135, DOWEC 10046_009, Petten, the Netherlands: Energy Research Center of the Netherlands, September 2003.

10. Lindenburg, C., "Aeroelastic Modelling of the LMH64-5 Blade," DOWEC-02-KL-083/0, DOWEC 10083_001, Petten, the Netherlands: Energy Research Center of the Netherlands, December 2002.
11. The UpWind Project. http://www.upwind.eu .
12. Jonkman, J., S. Butterfield, W. Musial, and G. Scott, "Definition of a 5-MW Reference Wind Turbine for Offshore System Development," NREL/TP-500-38060, Golden, CO: National Renewable Energy Laboratory, February 2009.
13. NWTC Design Codes (FAST by Jason Jonkman). http://wind.nrel.gov/designcodes/simulators/fast/. Last modified 12-August-2005; accessed 12-August-2005.
14. Personal communication, R.P.L. Nijssen, May 2009.
15. R. Gasch, J. Twele, Scaling wind turbines and rules of similarity, in: R. Gasch, J. Twele (Eds.), Wind Power Plants, Springer Berlin Heidelberg, 2012, pp. 257e271 (English).
16. Bisplinghoff, R.L and H. Ashley, "Principles of Aeroelasticity," Wiley and Sons, Inc., 1962.
17. Jonkman J, Butterfield S, Musial W, Scott G. Definition of a 5-MW reference wind turbine for offshore system development. *NREL/TP-500-38060*, 2007.
18. Structural steelwork. Analysis of safety against buckling of shells. *DIN 18800 Part 4*, 1990.
19. Chaviaropoulos PK. Similarity rules for W/T up-scaling. *UpWind Report, WP 1B4*, 2007.
20. Riziotis VA, Voutsinas SG, Politis ES, Chaviaropoulos PK, Hansen AM, Madsen AH, Rasmussen F. Identification of structural non-linearities due to large deflections on a 5

MW wind turbine blade. In *Proceedings of the 2008 European Wind Energy Conference and Exhibition*, Chaviaropoulos PK (ed.). EWEA: Brussels, 2008; 9–14.

21. Madsen AH, Rasmussen F. Influence of rotational sampling of turbulence in combination with up-scaling of wind turbine rotors, Note in WP2 of UpWind Project, 2010.
22. Jamieson P. Loading trends from certification calculations. *UpWind Report, WP 1B4*, 2007.
23. IEC 61400-1. *Wind Turbines: Part 1: Design Requirements*, (3rd edn). International Electrotechnical Commission: Geneva, Switzerland, 2005.
24. Chaviaropoulos PK, Lekou D, Sieros G. Cost models applied to blades. *UpWind Presentation, WP1B4*, Amsterdam,2010.
25. Powell MJD. A direct search optimization method that models the objective and constraint functions by linear interpolation. In *Advances in Optimization and Numerical Analysis, Proceedings of the Sixth Workshop on Optimization and Numerical Analysis*, Gomez S, Hennart J-P (eds). Kluwer Academic: Dordrecht, 1994; 51–67.
26. Sieros G, Chaviaropoulos PK. Upscaling beyond classical similarity: case study W/T tower. *UPWIND Project Report*, 2009.
27. Sieros G, Chaviaropoulos PK. Aspects of upscaling beyond similarity, *TORQUE 2010 conference*, FORTH, Heraklion,Crete, 2010; 63.
28. Malcolm DJ, Hansen AC. WindPACT turbine rotor design study. *NREL Report NREL/SR-500-32495*, 2002.
29. J. Manwell, J. McGowan, and A. Rogers. Wind Energy Explained. Theory, Design and Application. John Wiley and Sons Ltd., 2002.
30. A. Suzuki and A. Hansen. Generalized dynamic wake model for YawDyn. In AIAA 99–0041, 37th Aerospace Sciences Meeting and Exhibit, Reno, Nevada, USA, 1999.

31. D. J. Laino. AeroDyn: Aerodynamics analysis routines for horizontal-axis wind turbine dynamics analyses. See also URL https://nwtc.nrel.gov/AeroDyn.
32. H. Glauert. The analysis of experimental results in the windmill brake and vortex ring states of an airscrew. H.M. Stationery Office, 1926.
33. M. L. Buhl. A New Empirical Relationship between Thrust Coefficient and Induction Factor for the Turbulent Windmill State. Technical report, National Renewable Energy Laboratory, Golden, Colorado, USA, 2005. NREL/TP-500-36834.
34. H. Glauert. A General Theory of the Autogyro. H.M. Stationery Office, 1928.
35. C. Bak, A. Madsen, and J. Johansen. Influence from blade-tower interaction on fatigue loads and dynamics (poster), pages 394–397. WIP Renewable Energies, 2001.
36. B. D. Hibbs. HAWT Performance With Dynamic Stall. Technical report, Solar Energy Research Institute, Golden, Colorado, USA, 1986. STR-2732.
37. T. Burton, N. Jenkins, D. Sharpe, and E. Bossanyi. Wind Energy Handbook. John Wiley and Sons Ltd., 2002.
38. R. E. Gormont. A Mathematical Model of Unsteady Aerodynamics and Radial Flow for Application to Helicopter Rotors. Technical report, US Army Air Mobility Research and Development Laboratory, Philadelphia, Pennsylvania, USA, 1973. AD- 767240.
39. A. Bjorck, M. Mert, and H. A. Madsen. Optimal parameters for the FFA-Beddoes dynamic stall model. In 1999 European Wind Energy Conference, Nice, France, 1999.
40. H. Snel and J. G. Schepers. Engineering models for dynamic inflow phenomena. In 1991 European Wind Energy Conference, Amsterdam, Netherlands, 1991.
41. H. Snel and J. G. Schepers. Investigation and modelling of dynamic inflow effects. In 1993 European Wind Energy Conference, Lubeck, Germany, 1993.
42. D. M. Pitt and D. A. Peters. Theoretical predictions of dynamic inflow derivatives. Vertica, 1(5):21–34, 1981.

43. International Standard. International Electrotechnical Commission, 2009-02. IEC 61400-3 Edition 1.0.
44. ANSYS Inc. ANSYS. See also URL http://www.ansys.com/.
45. Dassault Systemes. Abaqus Unified FEA. http://www.3ds.com/productsservices/simulia/products/abaqus/.
46. Dassault Systemes. SolidWorks. http://www.solidworks.co.uk/.
47. Sandia National Laboratories, NuMAD, http://energy.sandia.gov/energy/renewableenergy/,wind-power/rotor-innovation/numerical-manufacturing-and-design-toolnumad/.
48. R. C. Juvinall and K. M. Marshek. Fundamental of Machine Component Design. John Wiley and Sons Ltd., 2012.
49. G. Bir. Pre-Processor for Computing Composite Blade Properties. See also URL https://nwtc.nrel.gov/PreComp.
50. M. E. Tuttle. Structural Analysis of Polymeric Composite Materials. CRC Press, 2012. Second Edition.
51. R. M. Jones. Mechanics of Composite Materials. McGraw-Hill, 1975.
52. O. A. Bauchau and J. I. Craig. Structural Analysis: With Applications to Aerospace Structures. Springer, 2009.
53. D. C. Sale. Co-Blade: Software for Analysis and Design of Composite Blades. See also URL https://code.google.com/p/co-blade/.
54. R. M. Rivello. Theory and Analysis of Flight Structures. McGraw-Hill, 1969.
55. D. H. Allen and W. E. Haisler. Introduction to Aerospace Structural Analysis. John Wiley and Sons Ltd., 1985.
56. D. J. Peery and J. J. Azar. Aircraft Structures. McGraw-Hill, 1982. Second Edition.

57. W. Young and R. Budynas. Roark's Formulas for Stress and Strain. McGraw-Hill, 2001. Seventh Edition.
58. T. Ashuri, M. Zaaijer, G. van Bussel, and G. van Kuik. An analytical model to extract wind turbine blade structural properties for optimization and up-scaling studies. In The Science of Making Torque from Wind, Crete, Greece, 2010.
59. G. Bir. BModes: Software for Computing Rotating Blade Coupled Modes. See also URL https://nwtc.nrel.gov/BModes.
60. G. Hayman. MLife: A MATLAB-based Estimator of Fatigue Life. See also URL https://nwtc.nrel.gov/MLife.
61. Astm international. Standard Practices for Cycle Counting in Fatigue Analysis, 2011. ASTM E1049 - 85(2011)e1.
62. M. A. Miner. Cumulative Damage in Fatigue. Journal of Applied Mechanics, 12(1):A159–A164, 1945.